



HAL
open science

Sustainable fabrication and pervaporation application of bio-based membranes: Combining a polyhydroxyalkanoate (PHA) as biopolymer and Cyrene (TM) as green solvent

Pacôme Tomietto, Francesca Russo, Francesco Galiano, Patrick Loulergue, Simona Salerno, Lydie Paugam, Jean-Luc Audic, Loredana de Bartolo, Alberto Figoli

► To cite this version:

Pacôme Tomietto, Francesca Russo, Francesco Galiano, Patrick Loulergue, Simona Salerno, et al.. Sustainable fabrication and pervaporation application of bio-based membranes: Combining a polyhydroxyalkanoate (PHA) as biopolymer and Cyrene (TM) as green solvent. *Journal of Membrane Science*, 2022, 643, pp.120061. 10.1016/j.memsci.2021.120061 . hal-03464807

HAL Id: hal-03464807

<https://hal.science/hal-03464807>

Submitted on 10 Dec 2021

HAL is a multi-disciplinary open access archive for the deposit and dissemination of scientific research documents, whether they are published or not. The documents may come from teaching and research institutions in France or abroad, or from public or private research centers.

L'archive ouverte pluridisciplinaire **HAL**, est destinée au dépôt et à la diffusion de documents scientifiques de niveau recherche, publiés ou non, émanant des établissements d'enseignement et de recherche français ou étrangers, des laboratoires publics ou privés.



Distributed under a Creative Commons Attribution - NonCommercial 4.0 International License

1 **Sustainable fabrication and pervaporation application of bio-based membranes:**
2 **combining a polyhydroxyalkanoate (PHA) as biopolymer and Cyrene™ as green solvent**

3
4 Pacôme Tomietto¹, Francesca Russo², Francesco Galiano^{2*}, Patrick Loulergue^{1*}, Simona
5 Salerno², Lydie Paugam¹, Jean-Luc Audic¹, Loredana De Bartolo², Alberto Figoli^{2*}

6 ¹ Univ. Rennes, Ecole Nationale Supérieure de Chimie de Rennes, CNRS, ISCR – UMR 6226, F-35000 Rennes,
7 France.

8 ² Institute on Membrane Technology (CNR-ITM), Via P. Bucci 17/c, 87036 Arcavacata di Rende, CS, Italy.

9 * Corresponding authors: f.galiano@itm.cnr.it; patrick.loulergue.1@univ-rennes1.fr; a.figoli@itm.cnr.it

10
11
12 **Abstract**

13 Within the prospect to develop a more sustainable solution for the membrane fabrication sector,
14 this work aims to investigate a new combination of bio-based materials, including a
15 polyhydroxyalkanoate (PHA) as a polymer and Cyrene™ as a solvent, for the phase inversion
16 process. The herein studied poly(hydroxybutyrate-co-hydroxyvalerate) (PHBHV) is a
17 microbial biopolymer with excellent biocompatible, biodegradable and solvent resistance
18 properties; while Cyrene™ is a non-toxic, biodegradable and renewable alternative to most of
19 the traditionally used polar aprotic solvents.

20 Several parameters of the phase inversion process were studied in order to identify the different
21 membrane microstructure possibilities and thus their final performances. The various studied
22 process parameters include the evaporation time before coagulation, the use of different
23 traditional and green additives, the concentration of polymer and additives into the dope
24 solution and the molecular weight of the additives. Polyethylene glycol (PEG),

25 polyvinylpyrrolidone (PVP) and an epoxidized broccoli vegetable oil (EBO) were successfully
26 used as pore former agents for these membranes. Developed membranes were fully
27 characterized in terms of morphology, topography, surface wettability, pore size, porosity,
28 thermal degradation, mechanical resistance and stability. After all, membranes exhibiting
29 different architectures (from porous to dense) were obtained. In order to prove their
30 applicability, dense membranes were finally successfully applied in pervaporation (PV) for the
31 separation of an organic/organic azeotropic mixture.

32

33 **Keywords:** bio-based membranes; PHBHV; CyreneTM; green solvents; biopolymers;
34 pervaporation

35 1 Introduction

36

37 In the last decades, the transition towards a circular economy, in order to face the current global
38 concerns, spurred to a shift in the production system from the use of petroleum-derived products
39 to the use of new chemicals deriving from renewable, recyclable and biodegradable resources.
40 Sustainable chemistry is at the basis of the new research of chemicals efficiently exploiting the
41 natural resources and minimizing carbon dioxide emissions and wastes production [1].

42 Pursuing the criteria of the process intensification strategy [2] and green chemistry design [3,4],
43 it is possible to develop and re-design new and more efficient processes which can operate with
44 a lower energy requirement and a reduced footprint tapping into natural raw materials.
45 Membrane operations, thanks to their numerous advantages, such as flexibility, low footprint,
46 modest energy requirement, simplicity of operation, absence of chemicals to achieve the
47 separation [2], well meet the needs of the sustainable development and process intensification
48 strategy. However, the way the membranes are produced still suffers from the use of chemicals
49 (polymer, solvents and additives) derived from fossil based sources or classified as toxic for
50 humans and harmful for the environment [5]. In order to establish a virtuous cycle, the entire
51 membrane process should be fully sustainable: starting from the preparation of the membrane
52 to its final disposal. Lawler et al. [6] studied, through a life cycle assessment, the environmental
53 impact of a reverse osmosis (RO) module used for water desalination, finding out that the
54 membrane production is the main contributor of CO₂ emissions to the atmosphere accounting
55 for the 45% of emissions for each module produced. Moreover, the materials employed for the
56 membrane preparation process (they considered polysulfone and polyamide as polymers
57 together with N,N-dimethylformamide (DMF) as solvent) are the components, during a RO
58 module manufacturing, with the highest negative impact on the environment in terms of
59 ecotoxicity, ozone and fossil depletion, marine and freshwater eutrophication. In addition, the
60 life cycle assessment of the fabrication of cellulose acetate membranes using N-methyl-2-

61 pyrrolidone (NMP) confirmed that the solvent has a major contribution on the overall
62 environmental impacts [7].

63 The choice of the proper polymer-solvent system is crucial in the formation of the membrane
64 and in determining the final morphology and properties. Currently, the most employed
65 polymers in porous membrane preparation, at laboratory and industrial scale, are polysulfone
66 (PSf), polyethersulfone (PES), polyvinylidene fluoride (PVDF), polytetrafluoroethylene
67 (PTFE) and polyacrylonitrile (PAN) which are all fossil-based materials. They are soluble in
68 traditional polar aprotic solvents, such as NMP, N, N-dimethyl acetamide (DMA) and DMF.
69 All these solvents, despite their large use in membrane manufacturing, can pose serious risks
70 for the environment and humans health. The USA Environmental Protection Agency (EPA),
71 for instance, recently proposed to ban NMP due to its possible reproductive toxicity, while
72 DMF and DMA are included in list of Substances of Very High Concern (SVHC) [8].

73 During the last years, a part of the research on membrane preparation started to shed the light
74 on new benign and green solvents which could be used for the preparation of polymeric
75 membranes and on reducing or abolishing the use of toxic solvents [9].

76 Seminal works started to explore a series of more sustainable or fully green solvents such as
77 triethyl phosphate (TEP) [10], dimethyl isosorbide (DMI) [11], Rhodiasolv® PolarClean
78 [12,13], ethyl lactate [14], *p*-Cymene [15] and Cyrene™ [16] to be used for the preparation of
79 more sustainable membranes using common polymers (e.g. PES and PVDF). Complementary
80 to the use of a green solvent, is the employment of sustainable materials such as biopolymers
81 able to provide a series of undoubtable benefits including biodegradability, biocompatibility,
82 easy processability, low cost and safe waste disposal [17]. The production of membranes based
83 on biopolymers is a growing field of interest and it is particularly attractive in biomedical and
84 pharmaceutical applications. Polylactic acid (PLA) [18], polybutylene succinate [19],
85 polyhydroxyalkanoates (PHA) [20–22], chitosan [23], alginate [24], cellulose acetate [25] and

86 starch [26] have been widely investigated as biopolymers for the production of membranes
87 applied in different sectors. However, biopolymers selection is not completely tailored for
88 membrane applications and their use is often challenging and problematic.

89 To fully respond to the requirements related to the reduction of waste generation and in
90 accordance with the basic principles of the Green Chemistry, this work aims to develop
91 innovative fully sustainable membranes exploiting raw bio-based materials (polymer, solvent
92 and additive) for targeted applications.

93 The biopolymer selected, poly(hydroxybutyrate-co-hydroxyvalerate) (PHBHV), is an
94 industrially available representative of the family of PHA, which are microbial biopolymers
95 with excellent biocompatible and biodegradable properties [27]. PHBHV is a linear copolymer
96 that is receiving growing attention due to its versatile thermomechanical properties tailored by
97 its hydroxyvalerate (HV) content [28,29].

98 PHBHV, moreover, differently from the most of the above-mentioned biopolymers, has the
99 advantage to be directly extracted from its biomass and displays remarkable organic solvents
100 resistance properties. In particular, PHBHV (especially when valerate content is low) is
101 generally soluble in chlorinated solvents but presents poor solubility in most common organic
102 solvents (e.g. ethanol, acetone, DMA, ethyl acetate or THF) under atmospheric pressure and at
103 moderate temperature [30,31].

104 After a preliminary evaluation screening carried out on different green solvents (e.g.
105 Tamisolve™, Rhodiasolv® PolarClean, dimethyl carbonate), dihydrolevoglucosenone
106 (Cyrene™) has been selected as the best option to solubilize PHBHV thanks to its ability to
107 completely solubilize the polymer and to form stable and homogenous dope solutions.
108 Cyrene™ is an innovative bio-based solvent derived from ligno-cellulosic biomass feed-stock
109 and produced by the Circa Group [32]. The synthesis of Cyrene™ occurs through the
110 intermediate 1,6-anhydro-3,4-dideoxy-D-glycero-hex-3-enopyranos-2-ulose (or

111 Levoglucosenone) that is converted into the final product by dehydrogenation [33]. Cyrene™
112 is a polar aprotic solvent with a chemo-physical profile comparable to traditional solvents
113 (NMP, DMA and DMF) [34]. Furthermore, Cyrene™ is non-toxic, biodegradable and
114 renewable. The most relevant physical-chemical properties and eco-toxicological information
115 of Cyrene™ respect to traditional solvents (NMP, DMF and DMA) are reported in Table S1.
116 In this work, the bio-based membranes were prepared by changing different phase inversion
117 parameters to evaluate the effect on membrane properties and performance. The influence of
118 polymer concentration, evaporation time and additives type was studied. The membranes have
119 been fully characterized in terms of morphology, topography, thickness, porosity, mechanical
120 properties, surface wettability and pure water permeability. The application of selected
121 membranes in pervaporation (PV) for the separation of a methanol (MeOH)/methyl tert-butyl
122 ether (MTBE) azeotropic mixture, at different operating temperatures, has been investigated.
123 Finally, long-term stability tests of two selected membranes were performed in sea water and
124 in enzymatic solution at room temperature and at 37°C, for up to 105 days, in order to assess
125 the membrane stability or microstructural changes overtime in aqueous medium.
126 To the best of our knowledge this is the first time that fully sustainable membranes, based on
127 polymers of the PHA family, are produced and characterized. This work aims to shed a new
128 light in a more and more sustainable and green preparation of polymeric membranes without
129 scarifying their properties and performance.

130

131 **2 Material and method**

132 2.1 Chemicals

133 PHBHV pellets were supplied by Tianan Biologic Material (China), under the trade name
134 Enmat Y1000P. They were purified by dissolution in chloroform and precipitation in methanol.
135 The white purified PHBHV powder was characterized by gel permeation chromatography
136 (GPC) equipped with three successive columns (2 × ResiPore and 1 × PL gel Mixed C from

137 Agilent) and a Waters UV detector working at a wavelength of 241 nm. The molecular weight
138 was determined to be 116 000 g.mol⁻¹. Differential scanning calorimetry (DSC) (TA
139 Instruments - Q10 DSC) was used to measure its crystallinity degree, $\chi_c = 62\%$, (see Fig. S1).
140 The crystallinity ratio (X_c) of the polymer was calculated based on the melting enthalpy
141 measured at the first cycle ($\Delta H_m = 89,99$ J/g). The following equation (Eq. 1) was used:

$$142 \quad X_c (\%) = (\Delta H_m / \Delta H_{PHB}^0) \times 100 \quad (1)$$

143 with $\Delta H_{PHB}^0 = 146$ J/g, the melting enthalpy of the polymer 100% crystalline.

144 The HV monomer content was determined by ¹H NMR analysis (Bruker 400 MHz) and was
145 equal to 2.3 mol%. This PHBHV has a T_g of 28 °C, a T_m of 172°C and a T_c around 120-130 °C.
146 Cyrene™ was used as the solvent and purchased from Sigma Aldrich. Conventional additives,
147 polyethyleneglycol (PEG) 200 g.mol⁻¹ (PEG200) and 600 g.mol⁻¹ (PEG600) were supplied by
148 Sigma Aldrich while polyvinylpyrrolidone (PVP) 17,000 g.mol⁻¹ (PVPK17) and 30,000 g.mol⁻¹
149 ¹ (PVPK30) were supplied by BASF.

150 Epoxidized broccoli oil (EBO) was investigated as a bio-based additive (see molecular structure
151 in supplementary information, Fig. S2) and it has previously been demonstrated to act as a
152 plasticizer for PHBHV [35].

153 It was produced by the epoxidation of a by-product generated during the manufacturing of a
154 food complement extracted from broccoli bean. EBO was gently provided by a research team
155 from the *Institut des Sciences Chimique de Rennes* [35]. It has a molecular weight of 1,017
156 g.mol⁻¹.

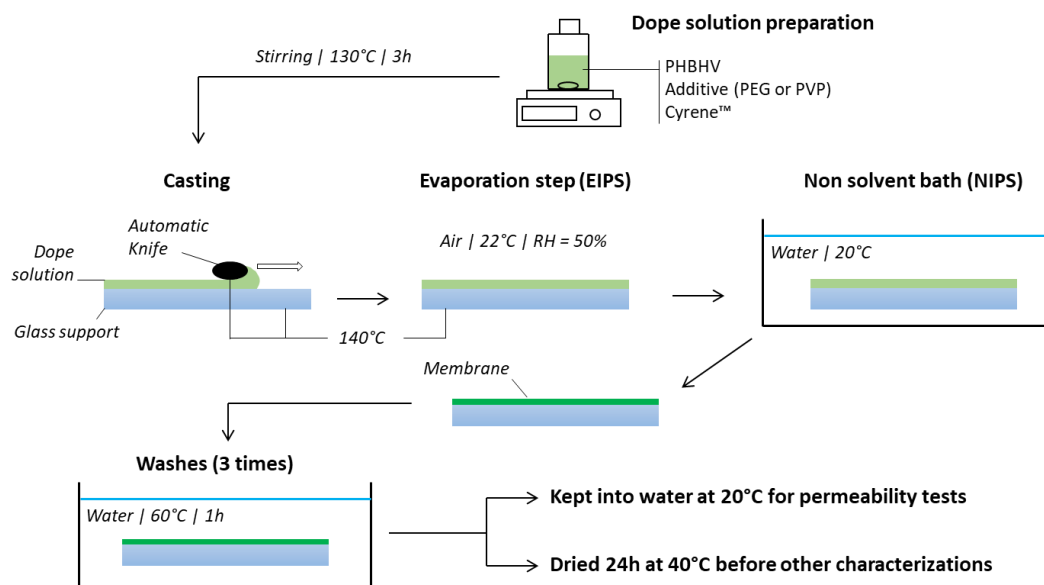
157 All the chemicals were used as received.

158 2.2 Membrane preparation

159 The schematic overview of the membrane fabrication is shown in Figure 1. First, dope solutions
160 were prepared by dissolving the additives and PHBHV into Cyrene™. The solutions were
161 stirred at 130°C for 3 hours. The different solution compositions of the fabricated membranes

162 are given in Table 1. The dope solutions were then automatically cast with a gap size of 300
 163 μm on a glass plate kept at 140°C and left for various delayed times (evaporation induced phase
 164 separation, EIPS step) before being coagulated in water (the environmental measured relative
 165 humidity (RH) was $50 \pm 4\%$). Then, the cast solutions were soaked into distilled water at 20°C
 166 to complete the phase inversion process by non-solvent induced phase separation (NIPS). Thus,
 167 the membranes were prepared by NIPS (when they were immediately immersed in water after
 168 casting) or by a combination of EIPS and NIPS when the evaporation step (from 0.5 to 5 min)
 169 was introduced before immersion in the coagulation bath (Table 1).

170 Afterward, to remove the remaining additives and solvent, the membranes were washed through
 171 three consecutive baths of distilled water at 60°C . Finally, the membranes were dried in an oven
 172 at 40°C for 24 hours (for measuring the water permeability the membranes were not dried but
 173 kept in water after preparation until their use).



174

175

Figure 1. A schematic overview of the membrane fabrication process.

176 The reference names and the fabrication parameters of the different membranes discussed in
 177 this study are shown in Table 1. The fabrication parameters that have been investigated include
 178 the dope solution composition (polymer and additive composition, additive nature) and the
 179 evaporation times.

180 **Table 1.** References and compositions of the various fabricated membranes. Concentrations
 181 are in weight percentage (wt%) in respect to the total dope solution.

Membrane reference	PHBHV concentration (wt%)	Additive		Evaporation time	Variable investigated
		Nature	Concentration (wt%)		
M-0				0	
M-0.5				0.5 min	Evaporation time
M-1.5	20%	None	/	1.5 min	
M-2.5				2.5 min	
M-5				5 min	
M-1.5-5PVPK17	20%	PVP17000	5%	1.5 min	
M-5-5PVPK17				5 min	
M-1.5-5PEG200	20%	PEG200	5%	1.5 min	
M-5-5PEG200				5 min	
M-1.5-5EBO	20%	EBO	5%	1.5 min	
M-5-5EBO				5 min	Additive and polymer concentration
M-1.5-7PEG200	20%		7%		
M-1.5-17/5PEG200	17%	PEG200	5%	1.5 min	
M-1.5-17/7PEG200	17%		7%		
M-1.5-17/7PVPK17		PVP17000			
M-1.5-17/7PVPK30	17%	PVP30000	7%	1.5 min	
M-1.5-17/7PEG600		PEG600			

182 The effect of EIPS before NIPS was studied through various evaporation times between 0 min
 183 and 5 min. The PHBHV concentration into the dope solution was between 17 wt% and 20 wt%.
 184 Various additives were investigated, including PEG200, PEG600, PVPK17, PVPK30 and EBO.

185 The concentrations of the additives into the dope solution that were investigated are 5 wt% or
186 7 wt%.

187 The tube tilting method was used to determine the sol-gel transition temperature for the
188 PHBHV/CyreneTM system. Different polymer concentrations (5, 10, 15 and 20 wt%) were, thus,
189 dissolved into the solvent at high temperature (130 °C). The temperature was, then, gradually
190 decreased (5°C every hour) until the gel phase was achieved.

191 The viscosity of dope solutions (20 wt% of polymer), prepared with and without additives (5
192 wt%), was measured at 90°C using a rotational rheometer (Brookfield, Synchro-Lectric
193 viscometer model: LV).

194 2.3 Characterization

195 2.3.1 Structural properties

196
197 The surface and cross section structures of each membrane were observed by SEM using a
198 Zeiss EVO, MA10. For the cross-section analyses, the samples were freeze-fractured in liquid
199 nitrogen. The samples were coated with a thin layer of gold prior analyses (sputter machine
200 Quorum Q 150R S).

201 Surface roughness of selected membranes was measured by means of atomic force microscopy
202 (AFM) (Bruker Multimode 8 with Nanoscope V controller). Data were acquired in tapping
203 mode, using silicon cantilevers (model TAP150, Bruker). The images were collected in a scan
204 size of 5 µm x 5 µm.

205 The average pore size of selected membranes was determined using a PMI Capillary Flow
206 Porometer (CFP1500 AEXL, Porous Materials Inc., USA) using the wet up/dry up method. The
207 membranes samples were initially wetted using Fluorinert FC-40 as a wetting liquid (surface
208 tension 26 dyne/cm) for 2 h.

209 The membrane porosity was calculated by means of the following equation (Eq. 2):

210
$$Porosity (\%) = \left(\frac{\frac{W_w - W_d}{\rho_k}}{\frac{W_w - W_d}{\rho_k} + \frac{W_d}{\rho_p}} \right) * 100 \quad (2)$$

211 where W_w is the weight of the wet membrane, W_d is the weight of the dry membrane, ρ_k is the
212 density of kerosene (0.80 g.cm^{-3}) and ρ_p is the density of the polymer (1.25 g.cm^{-3}). Three
213 pieces of each membrane were weighted before and after their immersion in kerosene for 24 h.

214 2.3.2 Physical-chemical and mechanical tests

215 The water contact angles of the membranes were evaluated on the top surfaces using ultrapure
216 water with the sessile drop method. The apparatus was a CAM200 instrument (KSV Instrument
217 LTD, Finland). The mean and standard deviation values were calculated with five
218 measurements.

219 The thermogravimetric experiments were carried out with a TGA Instruments SDT-Q600
220 apparatus at a scanning rate of $10^\circ\text{C.min}^{-1}$ under air with a temperature ramp from 20°C to
221 700°C .

222 The mechanical properties of the membranes were evaluated using a Zwick Roell Z 2.5
223 apparatus. Each sample was stretched unidirectionally at a steady velocity of 5 mm.min^{-1} . The
224 initial distance between the clamps was of 50 mm. The mean of three samples was performed.

225 2.3.3 Pure water permeability (PWP)

226 The PWP was evaluated using a typical laboratory cross-flow cell purchased from DeltaE
227 S.R.L. (Italy). Pure water at 20°C was pumped across the membrane (surface: 8 cm^2) by using
228 a gear pump (Tuthill Pump Co., California). First, the membranes were conditioned with a
229 transmembrane pressure of 2 bar until the water flow stabilized. Then, the PWP ($\text{L.m}^{-2}.\text{h}^{-1}.\text{bar}^{-1}$)
230 was calculated by means of the following equation (Eq. 3):

231
$$PWP = \frac{Q}{S \times TMP} \quad (3)$$

232 where Q is the water flux ($L \cdot h^{-1}$), S the membrane surface area (m^2) and TMP the
233 transmembrane pressure (bar).

234 2.3.4 Swelling experiments

235
236 The swelling degree of the dense membranes selected for the PV experiments was evaluated
237 into methanol (MeOH), methyl tert-butyl ether (MTBE) and a mixture of them (50/50 w/w).
238 First, small pieces of the membrane were weighed and introduced into each solvent solution.
239 The samples were then left at 30 °C for 48 h. Afterward, the swollen pieces were removed from
240 the solution, the excess of solvent on their surfaces was eliminated gently by using absorbent
241 paper and they were then directly weighed. Experiments were carried out using a digital
242 balance (Gibertini, Crystal 500, Italy) with the accuracy of 0.0001 g. The swelling degree for
243 each membrane was calculated using the following equation (Eq. 4):

$$244 \quad \text{Swelling degree (ml/g)} = \frac{1}{\rho_s} \left(\frac{W_w - W_d}{W_d} \right) \quad (4)$$

245 where ρ_s is the solvent density (MTBE: 0.74 g/ml; MeOH: 0.79 g/ml; MeOH/MTBE 50/50 w/w
246 0.765 g/ml), W_w is the weight of the wet piece and W_d is the weight of the dry piece. Swelling
247 was determined as described by Geens et al. [36].

248 2.3.5 Pervaporation (PV) experiments

249 The PV performance of selected membranes showing a dense morphology was studied for the
250 separation of a MeOH/MTBE organic/organic solution at the azeotropic point (MeOH/MTBE,
251 14.3/85.7, w/w).

252 The membrane cell of the laboratory scale set-up (see Fig. S3) was made of two stainless-steel
253 half-cylinders hermetically sealed with nuts and bolts between which the membrane was placed
254 on a porous stainless-steel plate. The effective surface of the membrane was 8.55 cm^2 . The cell
255 was equipped with a mechanical stirrer and was thermally regulated with a double jacketed
256 water circulation system. On the permeate side, the vapor was trapped into a glass condenser
257 cooled by liquid nitrogen. A vacuum of 0.5 ± 0.1 mbar was applied on the permeate side by

258 means of a rotary vane pump RV5 (Edwards) and it was monitored using an Active Pirani
259 Gauge (APG-M-NW16 AL, Edwards) manometer.

260 For each PV experiment, 200 mL of the azeotropic mixture were added into the cell and kept
261 at 25°C, 35°C or 45°C. Once the steady state was reached, permeate samples were collected on
262 a duration of at least 2h 30min. The total permeate flux J_t ($\text{Kg}\cdot\text{m}^{-2}\cdot\text{h}^{-1}$) was calculated as follows
263 (Eq. 5):

$$264 \quad J_t = \frac{\Delta m}{S \times \Delta t} \quad (5)$$

265 where Δm is the weight of the collected permeate (Kg), S the effective surface area of the
266 membrane (m^2) and Δt the permeate collection time (h).

267 The composition of the feed and permeate samples were determined by measuring their
268 refractive index with an Abbe 60DR refractometer (Bellingham and Stanley) at 25°C. The
269 membrane selectivity factor (α) was then calculated as follows (Eq. 6):

$$270 \quad \alpha = \frac{y_{\text{MeOH}}/y_{\text{MTBE}}}{x_{\text{MeOH}}/x_{\text{MTBE}}} \quad (6)$$

271 y_{MeOH} and y_{MTBE} are the respective concentrations of MeOH and MTBE into the permeate.

272 x_{MeOH} and x_{MTBE} are the respective concentrations of MeOH and MTBE into the feed.

273 2.3.6 Membrane degradation

274 The weight loss of two selected membranes in aqueous medium were assessed up to 105 days
275 by membrane incubation in sea water from the Tyrrhenian sea (south west of Italy) and in
276 enzymatic solution, both at 25°C and 37°C. The enzymatic solution was a fungal lipase from
277 *Candida Rugosa*, 150 $\text{U}\cdot\text{mL}^{-1}$ in phosphate buffered solution pH 7.4, with 0.01% NaN_3 . Before
278 the incubation, four different samples (2x2 cm) from each batch were dried in a vacuum oven
279 and their initial weight (W_i) exactly measured. Then the samples were immersed in 4 mL of sea
280 water or enzymatic solution, which were freshly changed every seven days. At the
281 predetermined time intervals, the samples were washed with copious distilled water, dried in

282 vacuum oven at 50°C for 4 hours, and their final weight (W_f) precisely measured. The
283 percentage of weight loss (W_{loss}) was determined by the following equation (Eq. 7):

284

$$285 \quad W_{loss} (\%) = \frac{W_f}{W_i} * 100 \quad (7)$$

286

287 The pH of all the aqueous media incubated with the membranes for the whole time was further
288 monitored.

289

290 **3. Results and discussion**

291 3.4 Membrane characterization

292 3.4.1 Effect of the evaporation time

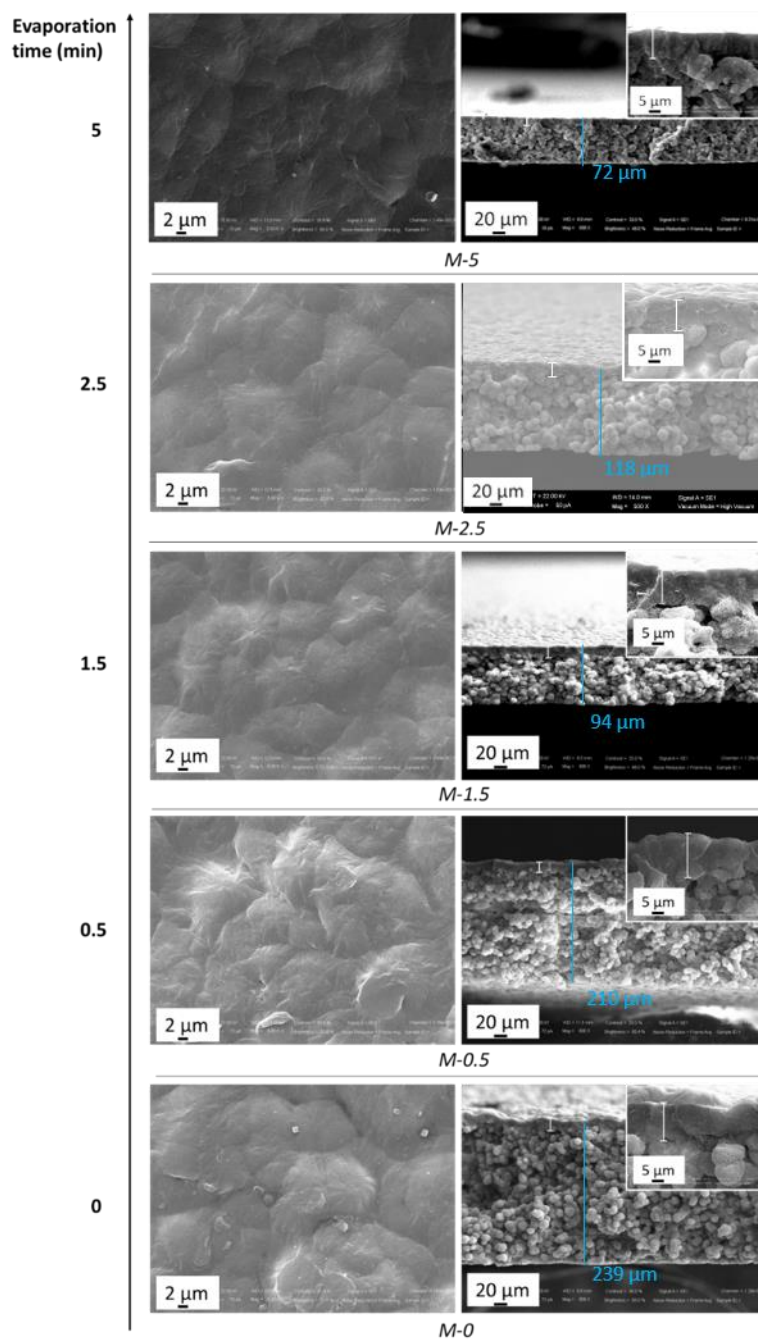
293 Preliminary tests started with the preparation of membranes resulting from a solution containing
294 20 wt% of PHBHV in Cyrene™, without any additive. The solutions, heated at 130°C, were
295 cast on a hot glass plate (140°C) and precipitated in water after an evaporation step ranging
296 from 0 (membrane prepared by NIPS) to 5 min (membranes prepared by EIPS+NIPS). The
297 heating of the glass plate was found to be crucial in order to prevent the premature gelification
298 of the solution before NIPS.

299 A polymer-solvent system is generally studied by means of a phase diagram in relation to cloud
300 point measurements at which a clear polymer solution becomes viscous and opaque [37]. This
301 phenomenon occurs as a consequence of the separation of a polymer-lean phase and a polymer-
302 rich phase (liquid-liquid phase separation). In our PHBHV/Cyrene™ system the solution
303 underwent a phase change (starting to form a viscous gel) as the temperature was decreased.
304 Fig. S4 shows the sol-gel transition temperature of the PHBHV/Cyrene™ system at different
305 polymer concentrations. The results indicate that the sol-gel transition temperature increased
306 (from 43 to about 70°C) as the polymer concentration increased (from 10 to 25 wt%). This can

307 be explained by the fact that a higher temperature is required to have a stable and homogenous
308 polymer solutions as the polymer concentration is increased.

309 The membrane prepared only by NIPS (M-0) revealed poor mechanical properties and a great
310 difficulty to be handled without breakage. The introduction of an evaporation step before
311 coagulation, on the contrary, was found to be very beneficial for improving the resistance of
312 the membranes. By looking at the cross-section morphology exhibited by the prepared
313 membranes (Figure 2) it is possible to observe, in fact, that the increase in the evaporation time
314 (from 0 to 5 min) led to a higher compactness especially for the evaporation time of 5 min for
315 which the spherulitic structure is not visible anymore resulting in more mechanically stable
316 membranes [38]. For the M-5 membrane, in fact, the spherulites seems fused together resulting
317 in a less porous membrane.

318



319

320 **Figure 2.** SEM images of the PHBV (20 wt%) based membranes prepared with different
 321 evaporation times before immersion in the coagulation bath. Top surface on the left and cross
 322 sections, with magnification and thickness measurements, on the right.

323 All the membranes display a smooth surface without visible pores or defects. The cross-
 324 sectional views showed dense upper structures, delimited by the white vertical line, associated

325 to spherulitic sublayers. The M-5 membrane differs slightly from the other membranes due to
326 a sublayer made of more aggregated spherulites.

327 The structure of the M-0 membrane, prepared only by NIPS, is characterized by a dense top
328 layer and a very porous spherulitic sublayer. The dense top surface is the result of a fast
329 solvent/non-solvent demixing and a rapid polymer precipitation occurring when the cast film is
330 put in contact with water [39]. This phenomenon is usually observed for the membranes
331 prepared by NIPS technique [39–41].

332 But then, once the top layer is formed, the solvent/non-solvent exchange rate is lowered, so that
333 the demixing in the sublayer is delayed. The spherulitic structure, observed for the sublayer, is
334 typical of membranes prepared by thermally induced phase separation (TIPS) technique with
335 (semi)crystalline polymers [37,41]. It is the result of a solid-liquid (S-L) demixing preceding
336 a sufficiently delayed liquid-liquid (L-L) demixing [42]. It is, moreover, favored in case of high
337 polymer concentrations or low coagulation bath temperatures [43]. In this case, the cast film
338 underwent a quick temperature change, from 140°C to 20°C, when introduced into the
339 coagulation bath, which induced a S-L demixing. This competition encountered between a
340 NIPS and a TIPS process has been previously observed and discussed for PVDF or PHBHV
341 membranes [21,41]. This observation indicates that the phase inversion process that occurred
342 during the fabrication of the membrane in this study is a hybrid TIPS-NIPS process.

343 When an evaporation step is introduced before the NIPS step, two other phase inversion
344 processes can start and potentially impact the final membrane structure: phase inversion *via*
345 intake of the air humidity (vapor induced phase separation, VIPS) or phase inversion *via* solvent
346 evaporation (EIPS). While VIPS involves, in most of the cases, a dominating non-solvent
347 (water) inflow, EIPS involves a non-solvent outflow. Hence, two major different structures
348 could be obtained.

349 In VIPS, the thermodynamic system, polymer/solvent/non-solvent, is the same as NIPS but
 350 with a slower demixing rate. Thus, the spinodal demixing does not occur and a porous structure
 351 without the dense upper layer is usually obtained [44]. On the contrary, in EIPS, the system to
 352 be considered is just a binary mixture polymer/solvent and a dense film would form through a
 353 S-L phase separation owing to solvent evaporation [45].

354 So, if the VIPS occurs during the evaporation time, a more porous top layer would be expected
 355 and if the EIPS occurs, a denser top layer would be foreseen. Both phenomena, actually, happen
 356 during this time interval with prevalence of one over the other depending on the balance
 357 between solvent outflow (EIPS) and non-solvent inflow (VIPS) [46]. For example, below a
 358 certain humidity level, the water intake rate would be too slow compared to the solvent
 359 evaporation rate and dense structures would be obtained [46].

360 In our case, increasing the evaporation time, a dense upper layer was always present, suggesting
 361 the absence of VIPS and the membrane formation by EIPS (Figure 2).

362 More details about the characteristic thicknesses of the membranes and their porosities are
 363 displayed in Table 2.

364 **Table 2.** Characteristics of the PHBHV based membranes made without additive and with
 365 different evaporation times.

	M-0	M-0.5	M-1.5	M-2.5	M-5
Evaporation time (min)	0	0.5	1.5	2.5	5
Thickness overall structure (μm)	239 ± 3	210 ± 4	94 ± 2	118 ± 3	72 ± 2
Dense upper structure (μm)	15 ± 2	15 ± 2	15 ± 2	16 ± 3	11 ± 1
Porosity (%)	<i>Not measurable Too fragile</i>	<i>Not measurable Too fragile</i>	70 ± 1	67 ± 3	43 ± 2
Water contact angle (°)	75 ± 2	74 ± 4	61 ± 1	69 ± 2	72 ± 4
Elongation at break (%)	1.3 ± 0.4	1.9 ± 0.1	2.0 ± 0.3	1.8 ± 0.3	3.3 ± 0.6

366

367 The overall membrane thickness varied from 72 μm, for the M-5 membrane, to 239 μm, for the
 368 M-0 membrane. The dense upper layer thickness varied from 11 μm to 16 μm among the
 369 membranes. The membranes prepared at the lowest evaporation times, M-0 and M-0.5, were

370 too fragile to make the porosity measurements possible. The other three membranes, M-1.5, M-
371 2.5 and M-5, displayed respective overall porosities of 70 %, 67% and 43%. This decrease in
372 porosity, as the evaporation time is increased, is clearly visible from the cross-section of the
373 membranes that shows more compact structure at higher evaporation times (Figure 2). In the
374 cross-section of the M-5 membrane, showing the lowest degree of porosity (43%), the
375 spherulites underneath the top layer are fused together making the overall membrane more
376 compact and less porous (as also evidenced by the lower membrane thickness (72 μm)).
377 These membranes displayed relatively hydrophilic surfaces with contact angle values ranging
378 from 61° to 75° . Since all the membranes have the same chemical composition, the variations
379 in contact angle values can be related to variations in their surface roughness which may depend
380 on their formation conditions [47].

381 AFM results (Fig. 3), carried out on M0, M1.5 and M5 membranes, in fact, confirm different
382 surface roughness for the investigated membranes. The topography of the membranes was
383 expressed in terms of root mean square (Sq), average roughness (Sa) and peak to peak value
384 (Sz). M0 displayed the higher values of roughness on its surface which can be responsible of
385 the highest value of contact angle exhibited by this membrane. The roughness is, in fact, related
386 to contact angle by the following equation (Eq. 8):

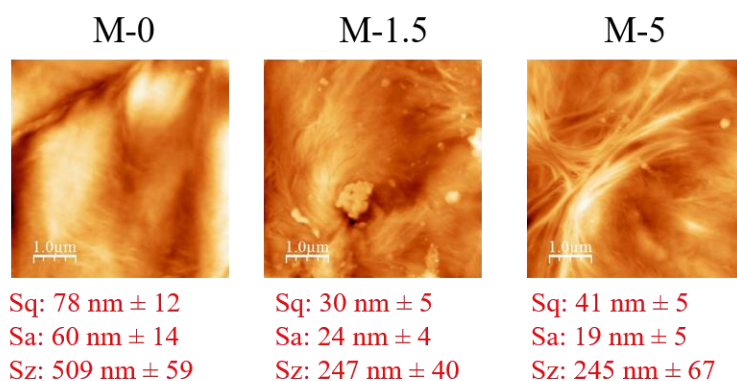
$$387 \quad \cos \theta_m = r \cos \theta_y \quad (8)$$

388 where r is the ratio of projected surface area to real surface area ($r = 1$ for a smooth surface and
389 $r > 1$ for a rough surface), and θ_y is the Young contact angle, which is equal to θ_m if $r = 1$ [48].

390 According to this equation the hydrophobicity of a membrane is reinforced by surface
391 roughness [49].

392 Therefore, the lower contact angle values shown by M1.5 and M5 membranes can be related to
393 their lower roughness degree respect to M0.

394



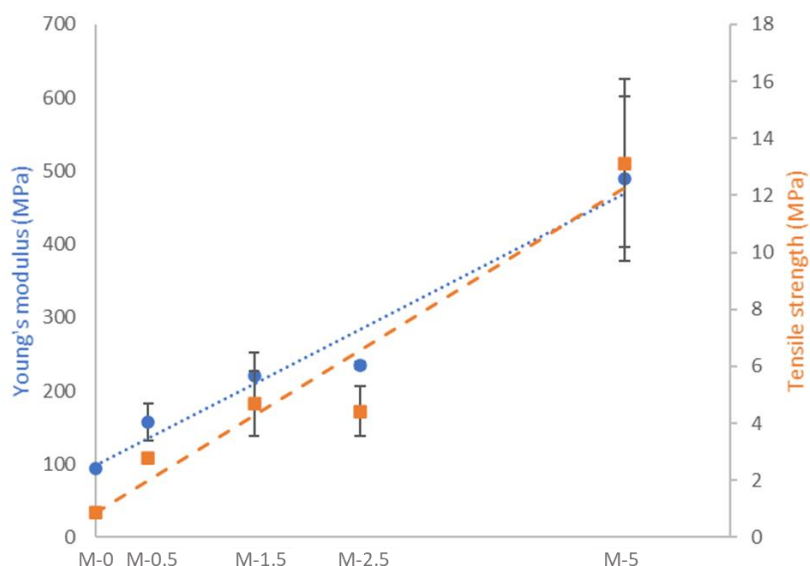
395

396 Figure 3. AFM images and roughness parameters of M-0, M-1.5 and M-5 membranes

397 It is also important to highlight that the wettability degree of PHBHV membranes reported in
 398 literature is not unanimous varying from hydrophobic values of 96° [50] to hydrophilic values
 399 of 76° and 72.5° [51,52]. These discrepancies could be related to the different content of HV in
 400 the polymer and to the topography of each membrane.

401 The mechanical properties of the investigated membranes are reported in Fig. 4.

402



403

404 **Figure 4.** Influence of the evaporation time on the mechanical properties of the PHBHV
 405 based membranes.

406 As expected, the Young's modulus and tensile strength of the membranes increased with the
 407 evaporation time, offering better mechanical properties. The Young's modulus varied from 94

20

408 MPa to 490 MPa while the tensile strength ranged from 0.87 MPa to 13 MPa. These results are
409 similar when compared to PVDF membranes which usually display a Young's modulus from
410 100 MPa to 600 MPa and a tensile strength from 0.2 MPa to 15 MPa [41,53].

411 The measured values of elongation at break (Table 2) are significantly lower than the ones
412 reported for PVDF or PSf membranes, usually between 10 % and 500 % [41,54,55]. The low
413 elongation at break is related to the properties of the used PHBHV, which has a crystallinity of
414 62% with rigid amorphous parts and a glass transition temperature of 28°C, responsible of the
415 fragility of the polymer [56,57].

416 The improvement of the mechanical properties, Young's modulus, tensile strength and
417 elongation at break is linked to the morphological changes induced by the introduction of the
418 evaporation step during membrane preparation. By increasing the evaporation time, more
419 interconnected spherulites are obtained (Figure 2), leading to lower porosities (Table 2) and
420 finally increasing the mechanical parameters. Voids and pores, in fact, represent weak points in
421 the polymer matrix making the membranes more fragile in comparison to denser structures [58].
422 The membranes exhibiting satisfying mechanical properties (M-1.5, M-2.5 and M-5) were
423 tested for PWP but none of them was permeable to water as consequence of their dense top
424 layer.

425

426 3.4.2 Effect of the dope solution composition

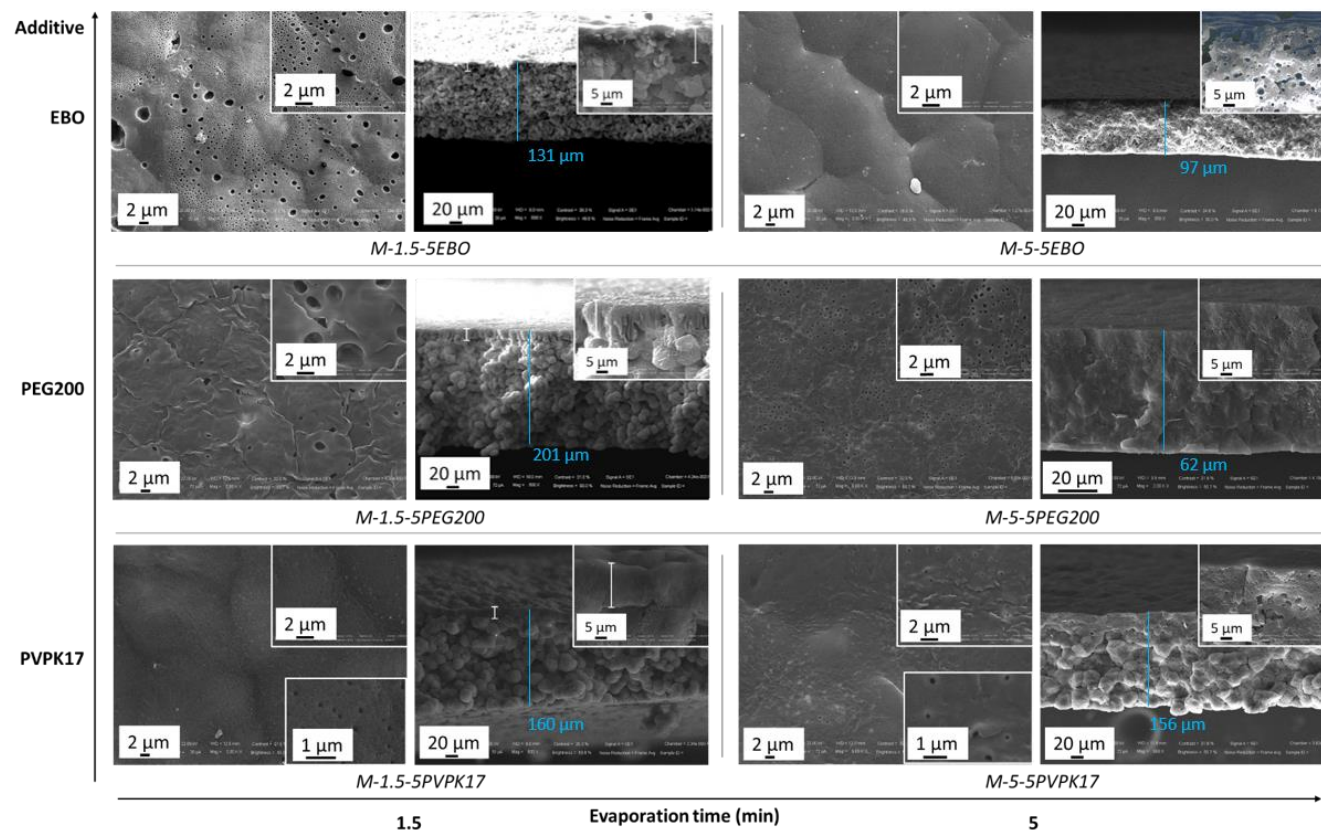
427 3.4.2.1 Nature of the additive

428 Within the prospect of tailoring the membrane microstructure and potentially membrane
429 performance, different additives, PEG200, PVPK17 and EBO, were included into the dope
430 solution. PEG and PVP have been both previously used for membrane fabrication with
431 Cyrene™ as a solvent [59]. They act as pore former and hydrophilic agents, enhancing the
432 water membrane permeability. PEG is a biodegradable, non-toxic compound with good

433 chemical and thermal stability. PVP is a fossil-based and non-toxic additive. On the other hand,
434 the EBO is a valorized co-product obtained from the synthesis of a food active ingredient,
435 already explored as a plasticizer for PHA based materials [35].
436 The PHBHV concentration was kept at 20 wt% and the additives concentration was fixed at 5
437 wt%. On the basis of the previous tests, two different evaporation times have been evaluated:
438 1.5 and 5 min. Below 1.5 min, in fact, the membranes demonstrated poor mechanical properties,
439 while 1.5 and 2.5 min produced membranes with similar structure and properties. The SEM
440 images of the membranes prepared with the three additives are shown in Fig. 5.

441

442



443

444 **Figure 5.** SEM images of the PHBV based membranes prepared with different additives and different evaporation times before immersion in
 445 the coagulation bath (dope solutions with 20 wt% PHBV and 5 wt% additive (PVPK17, PEG200 or EBO)). Top surface, with magnification,
 446 on the left and cross section, with magnification and thickness measurements, on the right.

447 For the membranes prepared with the three additives and an evaporation time of 1.5 min, M-
448 1.5-5PVPK17, M-1.5-5PEG200 and M-1.5-5EBO, the SEM images show porous surfaces with
449 a spherulitic sublayer visible along the cross-section as the results of the hybrid TIPS-NIPS
450 mechanism. Hence, the effect of the additives is clearly visible on the surfaces of the membranes
451 where pores with various sizes are present. The membrane with PEG200 as an additive, M-1.5-
452 5PEG200, is the only one with finger like macrovoids above the spherulitic part. This result can
453 be related to the lower MW of PEG200 (200 g.mol^{-1}) compared to EBO ($1,017 \text{ g.mol}^{-1}$) and
454 PVPK17 ($17,000 \text{ g.mol}^{-1}$), which affects the viscosity of the dope solution. Since the dope
455 solution viscosity increases with the additive molecular weight, the lower viscosity of the dope
456 solution with PEG200 could result in a faster L-L demixing promoting the formation of
457 macrovoids [60]. These results are, in fact, confirmed by viscosity measurements carried out
458 on the solutions prepared with and without additives. The lower viscosity value was found for
459 the dope solution formed by only polymer (20 wt%) and solvent which was 2461 cP. The
460 viscosity was increased as PEG200 (5 wt%) was added in the dope solution (5532 cP). A further
461 viscosity increase (6,539 cP) was, then, observed when PVPK17 (5 wt%) was used, as a
462 consequence of its higher molecular weight. Finally, the addition of EBO led to a drastic
463 increase in solution viscosity (88,511 cP) due to its high density.

464 It is also worth noting that EBO leads to the formation of more and larger surface pores
465 compared to PEG200 and PVPK17 (Fig. 5). However, the EBO membrane appears to have
466 the lowest porosity (Table 3). These observations are not contradictory as the SEM picture only
467 allows to observe surface pores while porosity measurements account for the whole membrane
468 volume including the upper and sublayers.

469 As previously observed, regardless of the nature of the additive, the overall membrane
470 microstructure tends to be less porous when the evaporation time is increased from 1.5 min to
471 5 min. For the M-5-5PEG200 and M-5-5EBO membranes, the spherulitic sublayer is not visible

472 anymore and it is replaced by a denser cross-sectional structure. The spherulitic substructure is
 473 still visible only for the M-5-5PVPK17 membrane, even if the spherulites seem to be fused
 474 together respect to the membranes prepared at 1.5 min. Some pores on the surface can be
 475 observed for the M-5-5PVPK17 and M-5-5PEG200 membranes.

476 Both the presence of additives and the evaporation time played a role in the EIPS process (Fig.
 477 5). From a thermodynamic point of view, additives can be compared to a non-solvent. In that
 478 case, the binary system polymer/solvent turns into the ternary system polymer/solvent/additive.
 479 Hence, during the solvent evaporation, instead of a direct S-L demixing, a L-L demixing,
 480 between a polymeric rich phase and an additive rich phase, can occur [45]. The additive rich
 481 phase would grow and coalesce to finally give the final pores of the membrane, herein observed
 482 on the surface, while the polymeric rich phase would yield to the membrane matrix.

483 More detailed characteristics of the membranes made with additives are displayed in Table 3.

484 **Table 3.** Characteristics of the PHBHV based membranes made with additives and different
 485 evaporation times.

	M-1.5- 5PVPK17	M-1.5- 5PEG200	M-1.5- 5EBO	M-5- 5PVPK17	M-5- 5PEG200	M-5- 5EBO
Evaporation time	1.5 min	1.5 min	1.5 min	5 min	5 min	5 min
Additive	PVPK17	PEG200	EBO	PVPK17	PEG200	EBO
Thickness overall structure (μm)	160 \pm 14	201 \pm 5	131 \pm 3	156 \pm 7	62 \pm 1	97 \pm 2
Upper structure (μm)	24 \pm 2	17 \pm 4	20 \pm 4	/	/	/
Water contact angle ($^\circ$)	70 \pm 2	63 \pm 3	84 \pm 1	74 \pm 7	70 \pm 1	75 \pm 1
Young's modulus (MPa)	120 \pm 48	187 \pm 45	71 \pm 4	457 \pm 91	300 \pm 35	419 \pm 51
Tensile strength (MPa)	1.4 \pm 0.5	1.7 \pm 0.4	1.8 \pm 0.3	21 \pm 5	11 \pm 3	8.6 \pm 0.7
Elongation at break (%)	2.0 \pm 0.5	1.7 \pm 0.4	1.3 \pm 0.1	3.1 \pm 0.1	3.0 \pm 1.0	4.1 \pm 2.3
Porosity (%)	70 \pm 2	67 \pm 1	61 \pm 1	48 \pm 2	52 \pm 4	44 \pm 4

486
 487 The overall membrane thickness ranged from 62 μm , for the M-5-5PEG200 membrane, to 201
 488 μm , for the M-1.5-5PEG200 membrane. The upper structure thickness was determined for the
 489 membranes showing well distinguished limits between the upper structure and the spherulitic
 490 sublayer. The upper structure varied from 17 μm to 24 μm among the membranes made with
 491 1.5 min evaporation time.

492 Despite the thickness differences, whether for the overall thickness or the upper structure
493 thickness, no clear trend is depicted with the additive nature or membrane porosity. One
494 potential explanation could be a variation of the closed porosity microstructure among these
495 membranes for the different additives tested. Indeed, since the closed cells can not be measured
496 with the porosity measurement technique employed here, it is possible that the closed porosities
497 among these membranes are different, thus what would impact the membrane thickness.

498 The surfaces of these membranes display a different hydrophilic character as demonstrated by
499 the water contact angles ranging from 63° to 84° . The membranes prepared with PEG200
500 revealed to be the ones with a more hydrophilic moiety respect to the membranes prepared with
501 EBO as an additive which presented the highest values of contact angle. PEG and PVP are
502 hydrophilic additives widely employed to improve the porosity and pore size of the membranes.
503 The measured contact angle values of the membranes prepared with these two additives are
504 slightly higher respect to pristine membranes (Table 2). This can be due to the different surface
505 topography of the membranes prepared with and without additives.

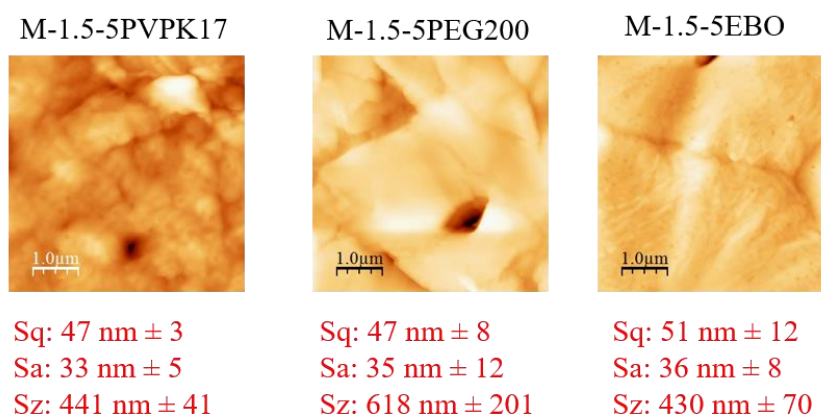
506 As evidenced from Fig. 6, in fact, the membranes prepared with PVP and PEG presented higher
507 values of S_q , S_a and S_z respect to the analogue membrane prepared without additives (M1.5).
508 The addition of PVP and PEG, in fact, promoted the formation of porous surfaces that,
509 according to Cassie-Baxter model, entrap more air pockets inside the pores inducing higher
510 contact angle values [61].

511 The higher contact angle value (84°) for the M-1.5-EBO membrane can be also related to its
512 higher values of roughness (S_q and S_a) with respect to the other membranes as a consequence
513 of the presence of large and numerous pores on its surface as evidenced in SEM images.

514

515

516

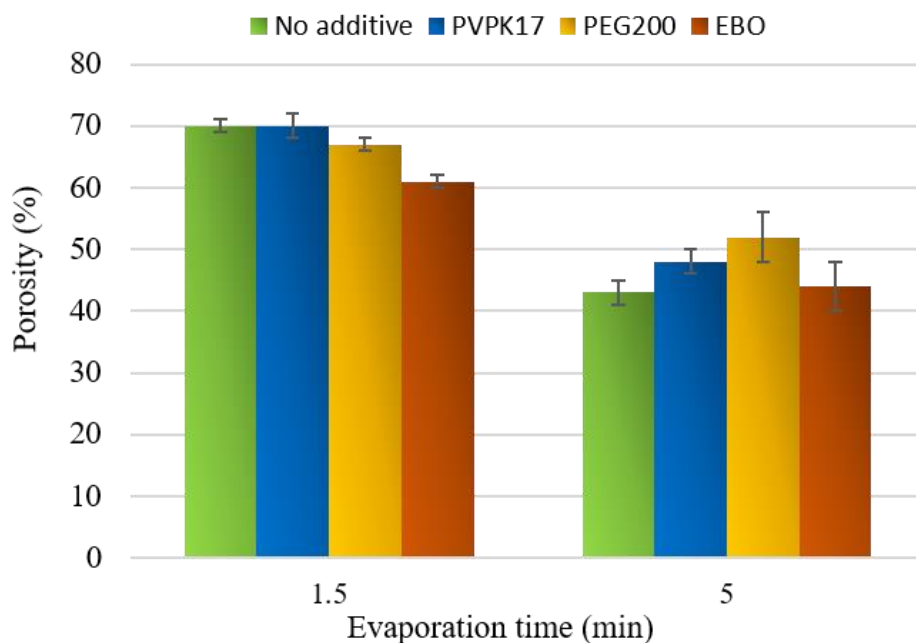


517

518 **Figure 6.** AFM images and roughness parameters of M-1.5-5PVPK17, M-1.5-5PEG200 and
519 M-1.5-5EBO membranes

520

521 The mechanical parameters, the Young's modulus, tensile strength and elongation at break were
522 enhanced when the evaporation was increased from 1.5 min to 5 min. Indeed, the Young's
523 modulus varied from 71 MPa to 187 MPa for the membranes obtained with 1.5 min of
524 evaporation time and from 300 MPa to 457 MPa for the membranes obtained with 5 min of
525 evaporation time. Coherently, both tensile strength and elongation at break risen significantly
526 with the evaporation time extension (Table 3). This is related to the decrease of porosity
527 observed at evaporation time of 5 min independently on the presence of additives (Fig. 7).



528
 529 **Figure 7.** Porosities of the PHBV based membranes as a function of the evaporation time
 530 (dope solutions with 20 wt% PHBV without additive (no additive) or with 5 wt% additive
 531 (PVPK17, PEG200 or EBO)).

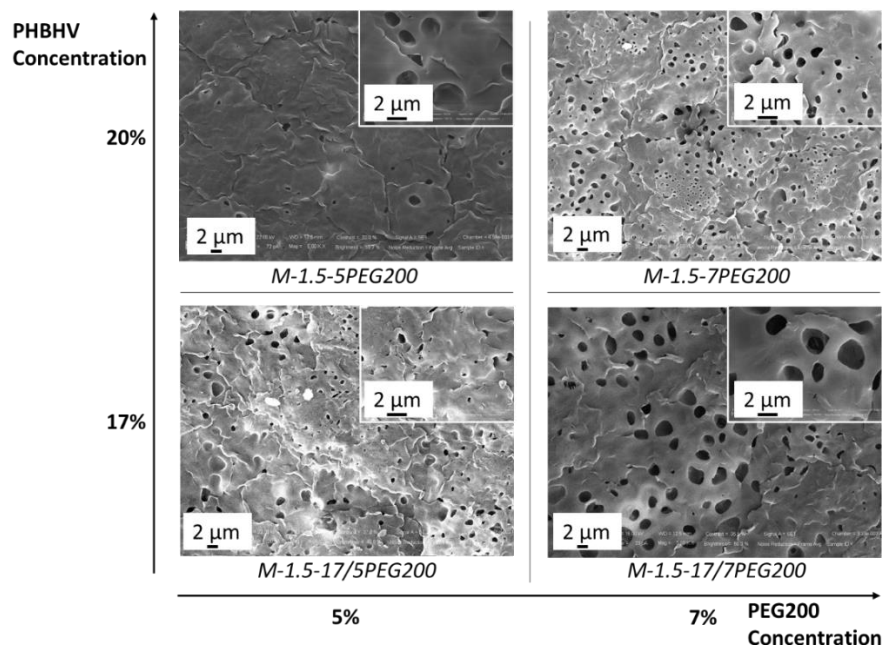
532
 533 PWP tests highlighted that only the M-1.5-5PEG200 membrane was permeable to water with a
 534 value of $200 \pm 80 \text{ L.m}^{-2}.\text{h}^{-1}.\text{bar}^{-1}$. This membrane combining large pores on its surface (Fig. 5)
 535 and high porosity (67 %) (Table 3) displayed a PWP value in the ultrafiltration (UF) range
 536 although highly variable. It should be also noted that the other membranes are not permeable to
 537 water suggesting the absence of open and interconnected pores.

538 3.4.2.2 Influence of polymer concentration, additives concentration and additives molecular 539 weight

540 The influence of the PHA concentration as well as additive concentration and molecular
 541 weights have been also investigated. To this purpose, the evaporation time was fixed at 1.5 min
 542 and PEG200 has been selected as a pore forming additive. The polymer concentration was
 543 lowered to 17 wt% meanwhile the additive concentration was increased to 7 wt%. Fig. 8

544 displays the surface SEM images of the PHBHV based membranes prepared by using different
545 polymer and PEG200 concentrations.

546



547

548 **Figure 8.** Top surface SEM images of the PHBHV based membranes prepared with different
549 polymer and additive (PEG200) concentrations (evaporation of 1.5 min).

550 All the membranes display a porous surface. When PEG200 concentration increases from 5%
551 to 7%, the size and number of surface pores increase. Similarly, when the PHBHV
552 concentration decreases from 20% to 17%, an increase of the size and number of pores is
553 observed. In other words, by decreasing the PHBHV concentration and increasing the additive
554 concentration, more and bigger pores over the surface can be observed without any variation in
555 the morphology of the cross-section that maintained a spherulitic substructure (see Fig. S5).

556 During the partial evaporation of the solvent at the surface, an increase of the additive
557 concentration enriches the additive phase volume, thus yielding more porous structures and
558 pores with bigger size. Moreover, from a kinetic point of view, the viscosity tends to decrease
559 with the reduction of the polymer/additive concentrations [62], which also favors the formation

560 and growing of the additive rich phase, thus encouraging the formation of pores. The Table 4
561 gives more details about the properties and PWP of these membranes.

562

563 **Table 4.** Characteristics of the PHBHV based membranes prepared with different
564 concentrations of PHBHV and PEG200 (evaporation time of 1.5 min).

	M-1.5- 5PEG200	M-1.5- 7PEG200	M-1.5- 17/5PEG200	M-1.5- 17/7PEG200
PHBHV Concentration	20 wt%	20 wt%	17 wt%	17 wt%
PEG200 Concentration	5 wt%	7 wt%	5 wt%	7 wt%
Thickness overall structure (μm)	201 ± 5	183 ± 5	323 ± 9	204 ± 21
Upper structure (μm)	17 ± 4	14 ± 5	17 ± 3	15 ± 3
Porosity (%)	67 ± 1	63 ± 2	74 ± 4	72 ± 1
Water contact angle ($^\circ$)	63 ± 3	67 ± 5	78 ± 5	63 ± 2
PWP ($\text{L}\cdot\text{m}^{-2}\cdot\text{h}^{-1}\cdot\text{bar}^{-1}$)	200 ± 80	12 ± 7	76 ± 21	21 ± 5

565

566 The overall membrane thickness ranged from 183 μm , for the M-1.5-7PEG200 membrane, to
567 323 μm , for the M-1.5-17/5PEG200 membrane.

568 With the 5 wt% PEG200 concentration, the membrane thickness increased from 201 μm to 323
569 μm when the PHBHV concentration decreased from 20 wt% to 17 wt%. This observation is in
570 good agreement with the higher porosity of the M-1.5-17/5PEG200 membrane (74%) compared
571 to the M-1.5-5PEG200 membrane (67%). Same trend can be observed for the membranes
572 prepared with the higher concentration of PEG200 (7 wt%).

573 Indeed, when the porosity increases, the number of voids inside the membrane microstructure
574 increases too, what finally favours a thicker membrane. Such increase of the membrane porosity
575 when the polymer concentration in the dope solutions decreases has previously been reported
576 [13,63].

577

578

579

580 Among these membranes, the upper structure varied from 14 μm to 17 μm , with very similar
581 values.

582 According to what has been observed in the SEM images (Fig. 8), the membrane porosity
583 increased when the polymer concentration decreased (from 20 to 17 wt%) for both
584 concentrations of additives employed (Table 4).

585 This behavior is in accordance with the results obtained with PVDF or cellulose acetate
586 membranes [13,63].

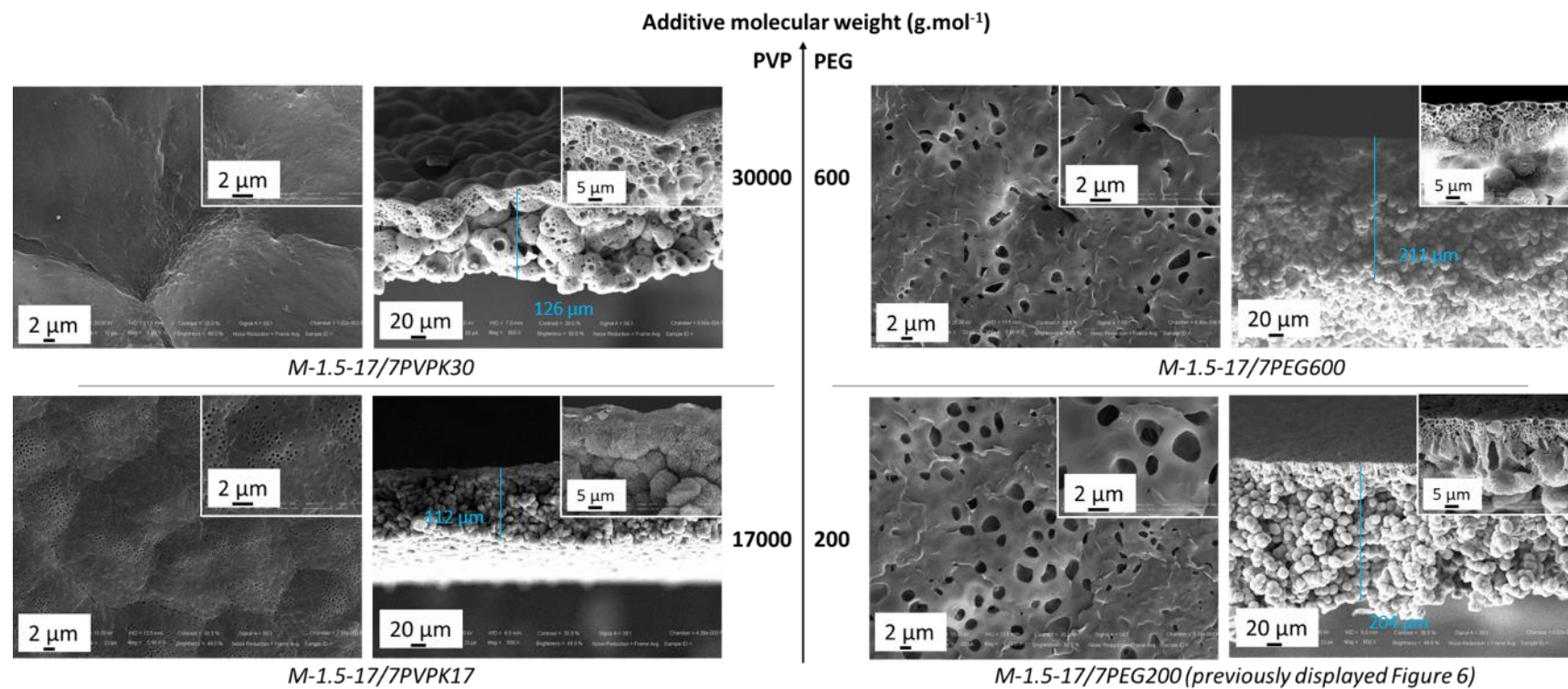
587 It is interesting to note that the increase of additive concentration from 5 wt% to 7 wt% did not
588 significantly influence the membrane porosity (Fig. 8). The membranes with 20 wt% of
589 PHBHV, M-1.5-5PEG200 and M-1.5-7PEG200, showed respective overall porosity values of
590 67% and 63% while the membranes with 17 wt% of PHBHV, M-1.5-17/5PEG200 and M-1.5-
591 17/7PEG200, gained a porosity of 74% and 72%, respectively. Usually, the increase in
592 concentration of a such additive would tend to increase the membrane porosity [41,54].
593 However, the additive might have a counter effect on the porosity since it increases the dope
594 solution viscosity [64,65]. Hence, it might be possible that the variation in PEG200
595 concentration from 5 wt% to 7 wt% would have hindered the internal porous network due to a
596 potential higher viscosity. These four membranes made from different PHBHV and PEG200
597 concentrations were all permeable to water.

598 However, no clear correlation can be depicted between the membrane permeability and the
599 membrane microstructure, which includes the membrane thickness, porosity and surface pores.

600 This could be the consequence of the formation of non-through pores (pore opened on one side
601 but closed on the other side). Thus, such pores would be visible on SEM pictures and considered
602 in the porosity determination by the gravimetric method (the pores are accessible through
603 diffusion when soaked into kerosene) but can not contribute to the permeate production as they
604 are closed on one side (i.e. water can not cross the membranes through these pores). In addition,

605 differences of pore tortuosity might exist for the different membranes. A more detailed analysis
606 of the membranes micro/nano structure using advanced methods such as micro/nano X-ray
607 tomography could help to elucidate the structure-performance relationships for such
608 membranes but was out of the scope of this study.

609 Finally, the impact of the PEG and PVP molecular weights on membrane properties has been
610 also investigated (Fig. 9). Previous studies, in fact, showed that the molecular weight of the
611 additive can greatly influence the thermodynamic and kinetic of the demixing process thus
612 affecting the membrane microstructure [54,66,67]. The increase of the molecular weight might,
613 for instance, enhances the membrane porosity [54,67], changes the macrovoids shape [67] or
614 hinder the formation of macrovoids [66]. By keeping PHBHV and additives concentrations
615 fixed at 17 wt% and 7 wt%, respectively, two different PVP and PEG molecular weights have
616 been considered: a 30,000 g.mol⁻¹ PVP (PVPK30) was compared to the 17,000 g.mol⁻¹ PVP
617 (PVPK17), while a 600 g.mol⁻¹ PEG (PEG600) was compared to the 200 g.mol⁻¹ PEG
618 (PEG200).



619

620 **Figure 9.** SEM images of the PHBV based membranes prepared with PVP or PEG of different molecular weights (dope solutions with 17 wt%

621 PHBV concentration and 7 wt% additive concentration with an evaporation time of 1.5 min). Top surface, with magnification, on the left and

622 cross section, with magnification, on the right.

623 SEM images of the top surfaces show a porous structure in all cases even if different pore sizes
 624 and densities are depicted. As seen before with other concentrations (Fig. 5), the PVP led to
 625 smaller pores on the surface compared to PEG. This is also confirmed by the mean pore
 626 diameter measurements performed on M-1.5-17/7PVPK17 and M-1.5-17/7PEG200
 627 membranes. Indeed, the membrane with PVP displayed a mean pore diameter of 0.04 ± 0.01
 628 μm while the membrane with PEG200 had a bigger mean pore diameter of $0.12 \pm 0.01 \mu\text{m}$.
 629 These results placed these membranes in the UF/MF range. For both PVP and PEG, when the
 630 additive molecular weight increased, the size of the surface pores seems to decrease. Indeed,
 631 the M-1.5-17/7PVPK30 and M-1.5-17/7PEG600 membranes have smaller pores than the
 632 respective M-1.5-17/7PVPK17 and M-1.5-17/7PEG200 membranes.

633 The cross-section views mainly reveal spherulitic structures for all the investigated membranes.
 634 A structure made of more aggregated spherulites is found in the membranes made with PVPK17
 635 or PVPK30 while M-1.5-17/7PVPK30 membrane exhibits closed cells within the upper layer
 636 and the spherulites. On the contrary, the membranes made with PEG200 or PEG600 show
 637 cellular structures on their upper parts. Table 5 gives more details about the structures and PWP
 638 results of these membranes.

639 **Table 5.** Characteristics of the PHBHV based membranes prepared with PVP or PEG of
 640 different molecular weights (Dope solutions with 17 wt% PHBHV concentration and 7 wt%
 641 additive concentration, with an evaporation time of 1.5 min).

	M-1.5- 17/7PVPK17	M-1.5- 17/7PVPK30	M-1.5- 17/7PEG200	M-1.5- 17/7PEG600
Additive nature	PVP	PVP	PEG	PEG
Additive molecular weight ($\text{g}\cdot\text{mol}^{-1}$)	17000	30000	200	600
Thickness overall structure (μm)	112 ± 8	126 ± 14	204 ± 21	211 ± 10
Upper structure (μm)	14 ± 2	32 ± 5	15 ± 3	14 ± 1
Porosity (%)	77 ± 1	56 ± 3	72 ± 1	73 ± 1
Water contact angle ($^\circ$)	75 ± 3	70 ± 2	63 ± 2	84 ± 2
PWP ($\text{L}\cdot\text{m}^{-2}\cdot\text{h}^{-1}\cdot\text{bar}^{-1}$)	37 ± 12	350 ± 93	21 ± 5	<i>Not measurable. Too fragile</i>

642

643 The overall membrane thickness varied from 112 μm , for the M-1.5-17/7PVPK17 membrane,
644 to 211 μm , for the M-1.5-17/7PEG600 membrane with an upper structure ranging from 14 μm
645 to 32 μm . Membranes show a similar porosity (72 % - 77 %) besides M-1.5-17/7PVPK30 that
646 exhibits a lower porosity (56%).

647 For the dope solutions using PVP, the overall membrane porosity decreased with the increase
648 of the additive molecular weight, as confirmed also by SEM images (Fig. 9). This behavior
649 could be due to a slower demixing that limits pores formation when the additive molecular
650 weight increases [62]. Indeed, the additives with lower molecular weights are prone to be more
651 easily leached out from the membrane during the coagulation in the water bath, what may favor
652 the increase of the overall membrane porosity [62].

653 The water contact angles of these four membranes, between 63° and 84° , still depicted the
654 hydrophilic behavior of the material.

655 The membrane PWP increased from $37 \text{ L}\cdot\text{m}^{-2}\cdot\text{h}^{-1}\cdot\text{bar}^{-1}$ to $350 \text{ L}\cdot\text{m}^{-2}\cdot\text{h}^{-1}\cdot\text{bar}^{-1}$ when the PVP
656 molecular weight increased from $17,000 \text{ g}\cdot\text{mol}^{-1}$ to $30,000 \text{ g}\cdot\text{mol}^{-1}$ accompanied also by an
657 improvement of membrane hydrophilicity. This increase in PWP can be attributed to the
658 increase in membrane average pore size (from $0.05 \pm 0.01 \mu\text{m}$ for M-1.5-17/7PVPK17 to 0.11
659 $\pm 0.01 \mu\text{m}$ for M-1.5-17/7PVPK30). The average pore size has been measured by using a
660 capillary flow porometer and thus directly relies on the extrusion of the wetting liquid from the
661 membrane pores. In other words, the pore size obtained by this technique is based on a fluid
662 permeability through the material and thus the measurement does not account for non-trough
663 pores.

664 Noteworthy, is that the pore size of both membranes, as shown in Fig. S6, has a very narrow
665 distribution for the M-1.5-17/7PVPK17 membrane (98% of the pores at $0.05 \mu\text{m}$) and a good
666 distribution for the M-1.5-17/7PVPK30 membrane (65% of the pores at $0.11 \mu\text{m}$).

667 The M-1.5-17/7PEG200 membrane showed a PWP of $21 \text{ L}\cdot\text{m}^{-2}\cdot\text{h}^{-1}\cdot\text{bar}^{-1}$ whereas the M-1.5-
668 17/7PEG600 was too fragile to be tested. Indeed, it has been observed that increasing the
669 concentration and molecular weight of the additive, the homogeneity of the membranes was
670 lost. A decrease of the additive solubility into the solvent (Cyrene™) could be the cause of
671 these observations.

672

673 3.5 Pervaporation results

674

675 The potentiality of the newly developed bio-based membranes has been demonstrated in PV
676 applications for the separation of organic/organic solutions. PHA based membranes, in fact,
677 have already shown their resistance towards a series of organic solvents and have been already
678 used in such applications [68]. The pervaporative performance of a selection of three of the
679 produced dense membranes were studied for the separation of a MeOH/MTBE mixture at the
680 azeotropic point (14.3/85.7 w/w). The influence of the additive nature and feed temperature on
681 the membranes' performances were investigated. The interest in separating such a mixtures lies
682 in the fact that an excess of MeOH is employed during the synthesis of MTBE, an octane
683 booster used in motor gasoline [69]. The advantage of PV, over conventional technologies such
684 as column distillation, consists in the possibility to break the forming azeotrope allowing the
685 complete separation of the organic/organic mixture.

686 The three selected membranes M-5, M-5-5PEG200 and M-5-5EBO are obviously not
687 permeable to water and exhibit a dense top layer or a dense cross-sectional structure (Figure 2
688 and Fig. 5). This makes them ideal to be employed in PV where dense membranes are required.
689 M-5 is the reference membrane that does not contain any additive. M-5-5PEG200 and M-5-
690 5EBO contain additives of different nature. The membranes are made from a 20 wt% PHBHV
691 concentration and 5 wt% concentration of additive (PEG200 and EBO) into the dope solution.
692 The three membranes display a moderate wettability as highlighted by water contact angles that

693 are 72°, 70° and 75° for the M-5, M-5-5PEG200 and M-5-5EBO membranes, respectively. The
694 hydrophilic character of these membranes would thus tend to favor the diffusion of MeOH
695 which is more polar than MTBE.

696 The Hansen Solubility Parameters (HSPs) of the chemicals involved during the separation
697 (membrane materials and solvents to be separated) and kinetic diameters of the solvents are
698 displayed in Table S2. The kinetic diameter of MeOH (0.40 nm) is lower than the one of MTBE
699 (0.62 nm), thus the MeOH is prone to diffuse faster through the membranes than the ether.
700 However, the solubility parameter δ_t of the polymer (20.6 MPa^{1/2}) is closer to the one of MTBE
701 (16.2 MPa^{1/2}) compared to MeOH (29.6 MPa^{1/2}), what means that the polymer has a better
702 predicted affinity with MTBE than MeOH and could hence favor the MTBE sorption and
703 diffusion.

704 When additives are involved, PEG200 ($\delta_t = 24.3$ MPa^{1/2}) may tend to increase the δ_t of the
705 overall material and thus its affinity with MeOH, while EBO ($\delta_t = 18.6$ MPa^{1/2}) would have the
706 opposite effect.

707 Swelling degree of the membranes was evaluated into three different solvent solutions: MeOH,
708 MTBE and the mixture MeOH/MTBE (50/50 w/w). The results are displayed in Fig. S7.

709 For each solvent solution, the M-5 membrane showed the lowest swelling degree (from 0.15 to
710 0.20 ml/g), followed by the M-5-5EBO membrane (from 0.14 to 0.28 ml/g) and, finally, by the
711 M-5-5PEG200 (from 0.16 to 0.37 ml/g). The swelling degree is in line with porosity values.
712 The higher degree of swelling of the M-5-5PEG200 membrane can be, in fact, related to its
713 higher porosity (52%). Thus, higher porosity leads to higher contact area between the
714 membrane and the solvent which promoted the adsorption of more solvent in the free volumes
715 of the membrane. While M-5 membrane, showing the lowest porosity value (43%), resulted in
716 the lowest swelling degree.

717 All the membranes swelled more in pure MTBE respect to pure MeOH in agreement with the
718 solubility parameter values. Interestingly, when MeOH and MTBE were used in mixture, the
719 swelling of the membranes was higher respect to the pure solvents, as also observed by S.
720 Zereshki et al. [70] for the same mixture (at 75 wt% of MeOH) with modified poly(ether ether
721 ketone) (PEEKWC) membranes.

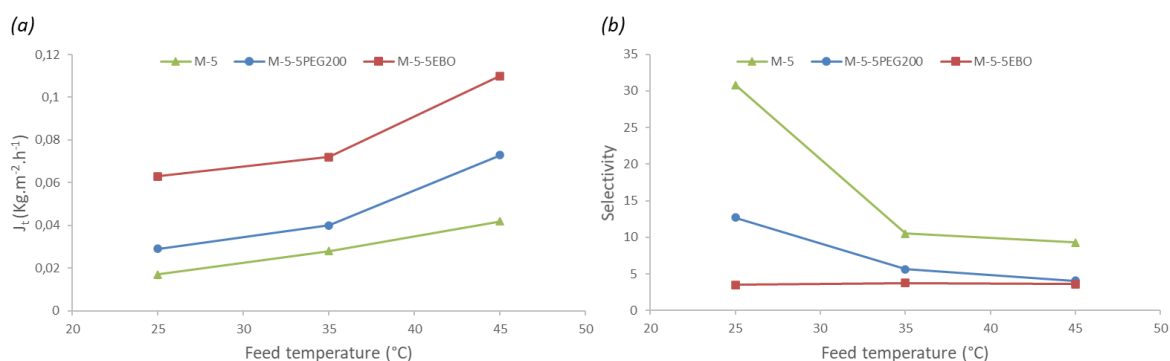
722 In order to investigate the thermal stability of the membranes, a thermogravimetric analysis
723 (TGA) was carried out up to 700°C and the obtained thermograms are plotted in Fig. S8.

724 The thermal degradation of M-5 membrane, without additive, occurs in one step with an onset
725 temperature of 270 °C. However, the M-5-5EBO membrane displays a two steps degradation
726 curve. The first temperature drop is associated to the PHBHV matrix whereas the second drop
727 is linked to the presence of EBO [35] into the membrane. For the M-5-5PEG200 membrane,
728 the degradation onset temperature is shifted down to 260 °C compared to the M-5 membrane.
729 This may be due to the remaining PEG200 that could decrease the degradation temperature of
730 the material. Finally, none of these membranes display a weight loss within the temperature
731 range used for the PV experiments (25 °C - 45 °C).

732 The same membrane sample, when tested in PV, at different feed temperatures (25°C, 35°C
733 and 45°C), did not show any visible alteration of its structure (cracks, wrinkles), for more than
734 one week (time necessary to the test the same sample at all investigated temperatures), as a
735 proof of its resistance and stability towards the investigated organic/organic solution.

736 Fig. 10 displays the membranes performances (total flux and selectivity) as a function of the
737 feed temperatures.

738



739

740 **Figure 10.** Effect of the feed temperature on: (a) the total permeate flux; and (b) the

741 selectivity for the three investigated membranes.

742 For all the membranes, as the feed temperature was increased, the flux increased (Fig. 10a)

743 while the selectivity decreased (Fig. 10b). The fluxes varied from 0.017 Kg.m⁻².h⁻¹ to 0.110

744 Kg.m⁻².h⁻¹ and the selectivity from 3.5 to 31. All the membranes were found to be selective for

745 MeOH showing a selectivity coefficient higher than 1. This could be explained considering two

746 aspects: 1) the smaller kinetic molecular diameter of MeOH (in comparison to MTBE) which

747 can allow its easier penetration through the membrane's free volumes; 2) the hydrophilic nature

748 of the PHBHV based membranes (as shown by contact angle measurements) able to favor the

749 permeation of more polar compounds such as MeOH.

750 The total flux and selectivity trend, observed in Fig. 10, is typical for PV. The flux increase is,

751 in fact, related to an increase in the thermal motion of membrane's polymer chains, which

752 promotes the formation of free volumes, favoring the permeation of more species [14].

753 Moreover, the increase in temperature, leads to a gain in the saturated vapor pressures of the

754 species in the feed side, which also foster their permeation through the membrane. However,

755 the larger free volumes, generated by the temperature increase, also facilitate the diffusion of

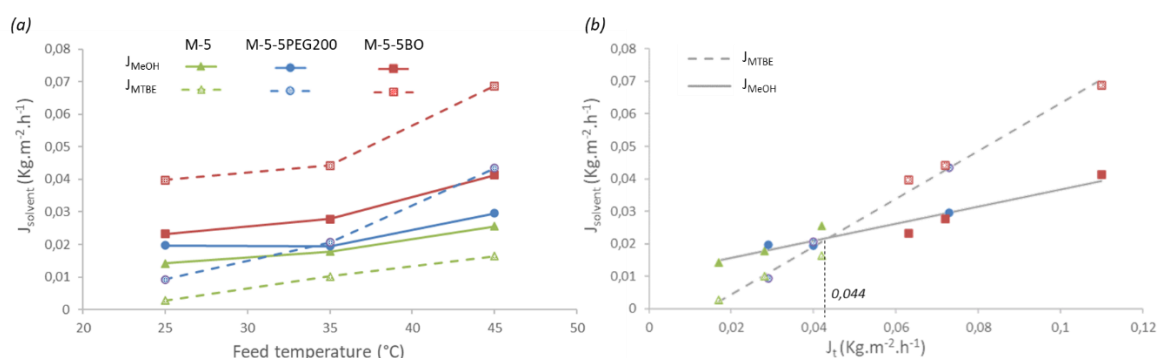
756 bigger molecules such as MTBE causing a decrease in membrane selectivity [71].

757 Analyzing the single behavior of each membrane, the M-5 membrane showed the lowest flux

758 and highest selectivity at all investigated temperatures. The presence of additives (PEG200 and

759 EBO) increased the flux of the membranes with a consequent decrease of selectivity. This effect

760 could be explained considering the plasticizing effect brought by the additives, what can favor
 761 the transfer of species, both MeOH and MTBE [72]. The EBO, in fact, has previously shown
 762 to be able to increase the free volume in PHA film materials [35]. This additive has a stronger
 763 impact on membrane performances in comparison to PEG200. In Fig. 11 the partial MeOH
 764 (J_{MeOH}) and MTBE (J_{MTBE}) fluxes are reported as a function of the feed temperature and the
 765 total permeate flux.



766
 767 **Figure 11.** MeOH (J_{MeOH}) and MTBE (J_{MTBE}) partial fluxes through the investigated
 768 membranes as a function of (a) the feed temperature (b) the total permeate flux.

769 For the M-5 membrane, the MeOH flux was always higher than the MTBE flux. The higher is
 770 J_{MeOH} compared to J_{MTBE} , the better is the selectivity. That is why M-5 shows the best selectivity
 771 (Fig. 10b). For the M-5-5PEG200 membrane, J_{MeOH} and J_{MTBE} intersect with each other at 35
 772 $^{\circ}C$.

773 Hence, at 45 $^{\circ}C$, J_{MTBE} becomes higher than J_{MeOH} . With this membrane, in fact, while the
 774 MeOH flux remained almost constant (from about 0.02 to about 0.03 Kg/m^2 h) with the
 775 temperature increase, the MTBE flux was greatly increased (from about 0.01 to about 0.045
 776 Kg/m^2 h) leading to a drop in membrane selectivity.

777 Then, in case of M-5-5EBO membrane, the MTBE flux was always higher than MeOH flux,
 778 what explains the lowest selectivity observed for this membrane (Fig. 10b).

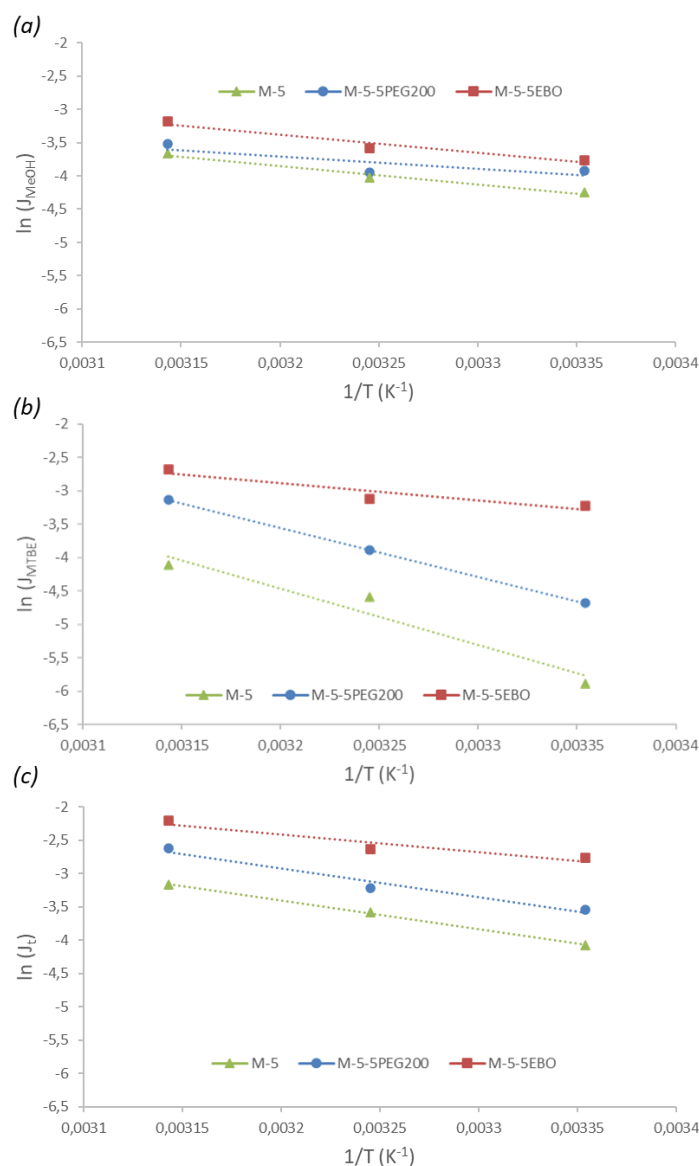
779 The Fig. 11b highlights the uneven linear variations of partial fluxes with the total permeate
 780 flux. Thereby, for a total flux of 0.044 $Kg.m^{-2}.h^{-1}$, the partial fluxes intersect with each other

781 and, at that point, J_{MTBE} starts to be higher than J_{MeOH} . It means that the higher is the total flux,
782 the higher is the amount of MTBE inside the permeate and the lower is the selectivity.
783 The fact that J_{MTBE} increases faster with the temperature than J_{MeOH} implies a more significative
784 dependency of MTBE on the temperature. This can be verified by calculating the fluxes
785 activation energies. The flux in PV usually follows an Arrhenius type relationship with the
786 temperature that can be expressed by the following equation (Eq. 9):

787
$$J_i = J_{0,i} \exp\left(-\frac{E_i}{RT}\right) \quad (9)$$

788 where J_i is the partial flux of the component i , $J_{0,i}$ is the pre-exponential factor (J_i flux at infinite
789 temperature) and E_i is the apparent activation energy for the component i . R is the ideal gas
790 constant and T the absolute temperature.

791 The sign of E_i shows the way the flux varies with the temperature whereas the absolute value
792 of E_i shows how much it depends on the temperature. In order to determine the activation
793 energies, the natural logarithms of fluxes ($\ln(J_i)$) are plotted according to the reciprocal
794 temperature in Fig. 12.



795
 796 **Figure 12.** Arrhenius plot of (a) the MeOH flux (J_{MeOH}), (b) the MTBE flux (J_{MTBE}) and (c)
 797 the total flux (J_t).

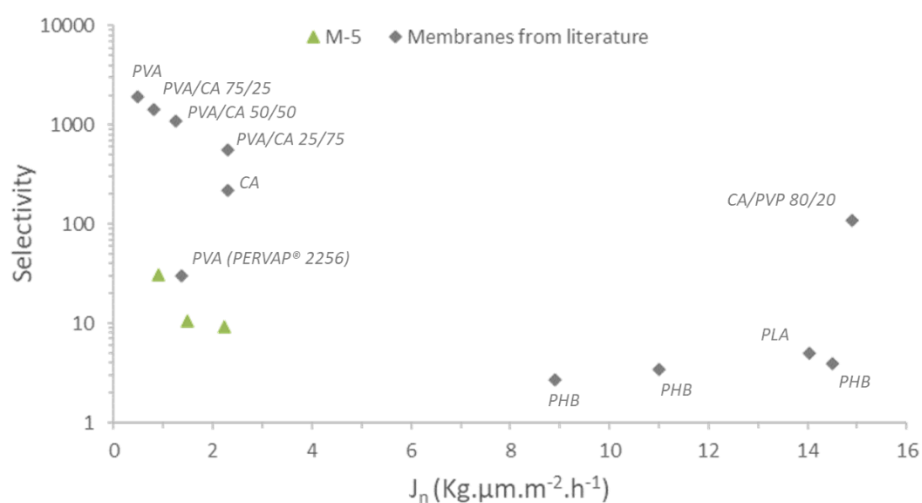
798 The obtained linear relationships indicate an Arrhenius dependence of fluxes with the
 799 temperature. The curves are decreasing in every case but the slopes are more pronounced for
 800 J_{MTBE} than for J_{MeOH} . In order to more clearly compare the dependencies, the activation energies
 801 are calculated according to these slopes and using the previous equation (Eq. 9). The obtained
 802 values are displayed in Table S3.

803 The positive values of the activation energies imply that fluxes increase with the increase of the
 804 feed temperature. For M-5 and M-5-5PEG200 membranes, the values for MTBE (respectively

805 70.6 KJ.mol⁻¹ and 60.8 KJ.mol⁻¹) are much higher than the ones of MeOH (respectively 23.0
 806 KJ.mol⁻¹ and 15.8 KJ.mol⁻¹), what means that MTBE flux increases more significantly than
 807 MeOH flux with the temperature. This phenomenon can be explained by an enlargement of the
 808 polymer free volume with temperature, which facilitates the passage of larger molecules such
 809 as MTBE [73]. On the other hand, for the M-5-5EBO membrane, the values are very similar
 810 between MTBE (21.4 KJ.mol⁻¹) and MeOH (22.6 KJ.mol⁻¹), explaining the low selectivity
 811 variation with the temperature increase (Fig. 10b).

812 Fig. 13 compares the performances of the M-5 membrane (the more selective one) with others
 813 extracted from the literature [72–77]. As the membranes from the different studies do not all
 814 have the same thickness, the selectivity has been plotted against the normalized flux to allow
 815 the direct comparison of the different membranes.

816



817

818 **Figure 13.** Representation of the performances, selectivity and normalized flux, of the herein
 819 fabricated PV membranes in comparison to membranes from the literature [72–77]. The
 820 MeOH concentration in feed varies from 14.3 to 20 wt%. The feed temperature varies from
 821 25°C to 50°C.

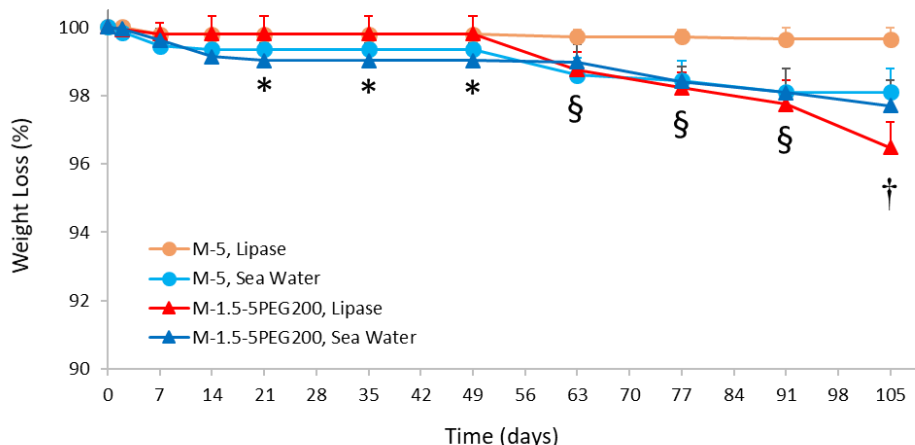
822 Compared to other biopolymer based membranes, the performances of these membranes are
 823 lower than polyvinyl alcohol (PVA) or cellulose acetate (CA) membranes, especially in regard

824 to their selectivity [72,74]. It may be explained by the more hydrophilic nature of these
825 polymers with regard to the PHBHV, what favors the transfer of polar molecules such as
826 MeOH. This is the reason why the blending of CA with PVA or PVP is a good way to improve
827 the membranes performances [72,74]. However, the M-5 membrane herein reported shows a
828 better selectivity in comparison to PLA and other polyhydroxybutyrate (PHB) based
829 membranes [73,76] and has similar values to the commercial membrane PERVAP® 2256 [75].

830 3.6 Biodegradability tests

831

832 The stability degradation into water-based environments of the M-5 and the M-1.5-5PEG200
833 membranes with different morphologies and properties was further assessed up to 105 days
834 (Fig. 14) by using sea-water at room temperature and an enzymatic solution of lipase from
835 *Candida Rugosa* (150 U.mL⁻¹) at 25°C and 37°C. Lipases, that are strongly studied for
836 industrial applications, catalyze the hydrolysis reaction of polyesters, such as polylactic acid,
837 polybutylene succinate and some PHA [78,79]. The active center of the lipase catalytic domain
838 have some amino acid sequences in common with PHA depolymerases [80]. The sea water
839 includes different compounds like dissolved salts, organic matters and microorganisms, and
840 represents the type of aqueous environment that the membrane would face for water filtration
841 applications.



842
 843 **Figure 14.** Weight loss (%) of M-5 and M-1.5-5PEG 200 membranes in aqueous medium by
 844 incubation in sea water and enzymatic solution of Lipase from *Candida Rugosa* (150 U mL⁻¹)
 845 over 105 days, at 25°C. Data statistically significant according to ANOVA followed by
 846 Bonferroni t'test ($p < 0.05$): (*) M-1.5-5PEG200 sea water vs M-5 lipase and M-1.5-
 847 5PEG200 lipase; (§) all vs M-5 lipase; (†) M-1.5-5PEG 200 lipase vs M-5 lipase and M-5 sea
 848 water, M-1.5-5PEG 200 sea water and M-5 sea water vs M-5 lipase.

849
 850 As displayed in Fig. 14, the M-5 membrane exhibits a weight loss of only $0.4 \pm 0.3\%$ and 1.9
 851 $\pm 0.7\%$, respectively, after 105 days in both lipase solution and sea water. The M-1.5-5PEG200
 852 membranes show a weight decrease of $0.97 \pm 0.5\%$ and $2.3 \pm 0.7\%$ after 21 and 105 days,
 853 respectively, in sea water. Same weight loss percentages were found for membranes incubated
 854 at the physiological temperature (data not shown). Coherently, the pH measures of all the
 855 aqueous media highlighted small fluctuations with time (Fig. S9), confirming the degradation
 856 results ~~good stability~~ of the tested membranes in aqueous solution.

857 The measured weight loss for the membranes into the lipase solution seems to be very low
 858 compared to what has been measured for similar PHBHV films in contact ~~more~~ PHA
 859 depolymerases [80]. A fast depolymerizing activity of different commercial lipases from
 860 fungal, bacterial and animal origin, has been observed for similar films P(3HB-co4HB) realized

861 with low polymer concentration (0.1%) [78,81]. In our work we used a polymer concentration
862 (20% PHBHV) of two order of magnitude higher than that reported in these studies. Indeed,
863 our results are in accordance with other reports that show a fairly slow degradation (5%) after
864 240 days of exposure in lipase solution for 2% PHBHV films [82,83], confirming a direct
865 correlation of the biodegradation rates with the polymer concentration.

866 For the sea water environments, the weight loss is also relatively low compared with other tests
867 into the real environment of sea water where the weight loss can be 7-20 % after 50-60 days
868 [84,85]—under variable conditions (e.g. temperature variations, potential mechanical stress,
869 constant microorganisms renewal or UV expositions). ~~are omitted.~~

870 Differently, our findings are in agreement with those reported for the biodegradation of a 10%
871 PHB film, that in static seawater collected from the Pacific Ocean, controlled at 25°C and
872 replaced every 2 days, lost 9% of the initial weight after 10 weeks [86].

873 The only case differing from the others is the M-5 Lipase, where the membrane weight seems
874 much more stable consistently with the dense structure of the membrane.

875 Finally, the membranes were extracted from their degradation environments after 105 days and
876 were analyzed by SEM (Fig. S10).

877 The surface of the M-1.5-5PEG200 and M-5 membranes was not greatly altered after 105 days
878 of ageing into the lipase solution. However, both membranes, after ageing into the sea water-
879 based solution tended to get more pores and rougher surfaces. Consequently, the sea water-
880 based solution seems to have an effect on the polymeric structure.

881 The sea water-based solution, however, contains a wide variety of bacteria, including the PHA
882 degrading ones, what would favor the biodegradation rate compared to the lipase solution.

883 These surface changes are actually due to the erosion via enzyme catalyzed hydrolysis [78].

884 During the biodegradation mechanism, first the microorganisms attach to the material surface
885 and then start the depolymerization through the enzyme catalyzed hydrolysis [87]. These two

886 first steps induce the measured weight loss. Afterward, the bacteria bio-assimilate and
887 mineralize the produced small molecules. Both surface or bulk erosion can occur, however, the
888 surface erosion may be predominant for semi-crystalline polymers, what can explain what is
889 obtained in this case. In the case of the lipase solution environment, because the material
890 morphology does not seem to be impacted after 105 days of ageing, catalyzed hydrolysis with
891 less specific enzymes, like Lipases, appear very low. Thus, the non-catalyzed hydrolysis of this
892 material would be even slower.

893 At the end, if the weight losses of the membranes within the different investigated environments
894 remain quite low although the sea water-based solution seems to impact the surface
895 morphology. This could influence the long-term performance of the membrane in the
896 perspective of water filtration application in an environment containing lipase enzyme opens a
897 new perspective in the application of these membranes in the filtration of aqueous solutions
898 containing known components.

899

900

901 **4 Conclusions**

902 This work aimed to develop a more sustainable and innovative way for the fabrication of
903 polymeric membranes by phase-inversion technique by exploiting a new combination of bio-
904 based materials, PHBHV as the polymer matrix and Cyrene™ as a green solvent. Asymmetric
905 membranes with suitable mechanical properties were successfully obtained by introducing a
906 pre-evaporation (EIPS) step before the coagulation bath. Besides the improvement of the
907 mechanical properties, this EIPS step also strongly influenced the membrane morphology,
908 including its cross-sectional microstructure and overall porosity.

909 A systematic study was, then, carried out by analyzing the impact of different variables, such
910 as: polymer concentration, additive concentration, additive nature and additive molecular
911 weight. In that prospect, PEG, PVP and a vegetable-based additive, EBO, were added as
912 hydrophilic and pore former agents into the dope solution. Thanks to them, more diversified
913 membrane microstructures were observed, including membranes with porous surfaces.

914 The different membranes architectures obtained resulted in membranes permeable to water (up
915 to $350 \text{ L}\cdot\text{m}^{-2}\cdot\text{h}^{-1}\cdot\text{bar}^{-1}$), with a pore size in the range of UF/MF, and in asymmetric membranes
916 displaying a dense top layer.

917 These latter ones, thanks to the solvent resistance properties of PHBHV, were applied in PV
918 for the separation of a MeOH/MTBE organic mixture at its azeotropic point.

919 All the three membranes resulted selective for MeOH as a consequence of their hydrophilic
920 nature and of the small dimension of the alcohol molecule. When PEG200 and EBO were used,
921 the selectivity decreased (in comparison to the membrane prepared without any additive) due
922 to their plasticizing effect in the membrane matrix which also resulted in a permeate flux
923 enhancement. The performance of most the performing membrane here produced was found to
924 be comparable (or even better) respect to other bio-based membranes made of PLA or PHB.

925 Porous and dense membranes showed also interesting stability performance when tested under
926 specific degradation environments for long periods of time, suggesting possible applications
927 for aqueous solutions filtration.

928 **5 Conflicts of interest**

929 There are no conflicts to declare.

930 **6 Acknowledgements**

931 This study was carried out in the framework of the PHC GALILEO 2020-2021 project
932 N°44342UM funded by the Ministero dell'Istruzione, dell'Università e della Ricerca (MIUR),
933 Ministère de l'Europe et des Affaires étrangères (MEAE), Ministère de l'Enseignement
934 supérieur, de la Recherche et de l'Innovation (MESRI), Campus France and by Università Italo
935 Francese (project G20_335). Pacôme Tomietto acknowledges Rennes Métropole for providing
936 the mobility grant making possible the collaboration between the two institutes involved in this
937 work.

938 The authors thank Dr. Claudia Ursino (Institute on Membrane Technology, ITM-CNR) and Dr.
939 Maria Penelope De Santo (Department of Physics, University of Calabria) for the AFM
940 measurements.

941

942 **References**

- 943 [1] R.A. Sheldon, Metrics of Green Chemistry and Sustainability: Past, Present, and
944 Future, ACS Sustain. Chem. Eng. (2018).
945 <https://doi.org/10.1021/acssuschemeng.7b03505>.
- 946 [2] E. Drioli, A.I. Stankiewicz, F. Macedonio, Membrane engineering in process
947 intensification-An overview, J. Memb. Sci. 380 (2011) 1–8.
948 <https://doi.org/10.1016/j.memsci.2011.06.043>.
- 949 [3] A. Figoli, T. Marino, S. Simone, E. Di Nicolò, X.-M. Li, T. He, S. Tornaghi, E. Drioli,
950 Towards non-toxic solvents for membrane preparation: a review, Green Chem. 16
951 (2014) 4034. <https://doi.org/10.1039/C4GC00613E>.
- 952 [4] P.T. Anastas, J.C. Warner, Green Chemistry: Theory and Practice, 1998.
953 <https://doi.org/10.1039/b513020b>.
- 954 [5] F. Russo, F. Galiano, A. Iulianelli, A. Basile, A. Figoli, Biopolymers for sustainable
955 membranes in CO₂ separation: a review, Fuel Process. Technol. (2020) 106643.
956 <https://doi.org/10.1016/j.fuproc.2020.106643>.
- 957 [6] W. Lawler, J. Alvarez-Gaitan, G. Leslie, P. Le-Clech, Comparative life cycle
958 assessment of end-of-life options for reverse osmosis membranes, Desalination. 357
959 (2015) 45–54. <https://doi.org/10.1016/j.desal.2014.10.013>.
- 960 [7] F. Prézéus, L. Tiruta-Barna, C. Guigui, J.-C. Remigy, A generic process modelling –
961 LCA approach for UF membrane fabrication: Application to cellulose acetate
962 membranes, J. Memb. Sci. 618 (2021) 118594.
963 <https://doi.org/10.1016/j.memsci.2020.118594>.
- 964 [8] United States Environmental Protection Agency, Risk Evaluation for N-

- 965 methylpyrrolidone (NMP), (n.d.). [https://www.epa.gov/assessing-and-managing-](https://www.epa.gov/assessing-and-managing-chemicals-under-tsca/risk-evaluation-n-methylpyrrolidone-nmp-0)
966 [chemicals-under-tsca/risk-evaluation-n-methylpyrrolidone-nmp-0](https://www.epa.gov/assessing-and-managing-chemicals-under-tsca/risk-evaluation-n-methylpyrrolidone-nmp-0).
- 967 [9] L. Pasetta, C. Echaide-Górriz, C. Téllez, J. Coronas, Vapor phase interfacial
968 polymerization: a method to synthesize thin film composite membranes without using
969 organic solvents, *Green Chem.* 23 (2021) 2449–2456.
970 <https://doi.org/10.1039/D1GC00236H>.
- 971 [10] T. Marino, F. Russo, A. Figoli, The Formation of Polyvinylidene Fluoride Membranes
972 with Tailored Properties via Vapour/Non-Solvent Induced Phase Separation,
973 *Membranes (Basel)*. 8 (2018) 71. <https://doi.org/10.3390/membranes8030071>.
- 974 [11] F. Russo, F. Galiano, F. Pedace, F. Aricò, A. Figoli, Dimethyl Isosorbide As a Green
975 Solvent for Sustainable Ultrafiltration and Microfiltration Membrane Preparation, *ACS*
976 *Sustain. Chem. Eng.* 8 (2020) 659–668.
977 <https://doi.org/10.1021/acssuschemeng.9b06496>.
- 978 [12] C. Ursino, F. Russo, R.M. Ferrari, M.P. De Santo, E. Di Nicolò, T. He, F. Galiano, A.
979 Figoli, Polyethersulfone hollow fiber membranes prepared with Polarclean® as a more
980 sustainable solvent, *J. Memb. Sci.* 608 (2020) 118216.
981 <https://doi.org/10.1016/j.memsci.2020.118216>.
- 982 [13] H.H. Wang, J.T. Jung, J.F. Kim, S. Kim, E. Drioli, Y.M. Lee, A novel green solvent
983 alternative for polymeric membrane preparation via nonsolvent-induced phase
984 separation (NIPS), *J. Memb. Sci.* 574 (2019) 44–54.
985 <https://doi.org/10.1016/j.memsci.2018.12.051>.
- 986 [14] F. Galiano, A.H. Ghanim, K.T. Rashid, T. Marino, S. Simone, Q.F. Alsalhy, A. Figoli,
987 Preparation and characterization of green polylactic acid (PLA) membranes for
988 organic/organic separation by pervaporation, *Clean Technol. Environ. Policy*. 21

- 989 (2019) 109–120. <https://doi.org/10.1007/s10098-018-1621-4>.
- 990 [15] S.-H. Park, A. Alammari, Z. Fulop, B.A. Pulido, S.P. Nunes, G. Szekely, Hydrophobic
991 thin film composite nanofiltration membranes derived solely from sustainable sources,
992 *Green Chem.* 23 (2021) 1175–1184. <https://doi.org/10.1039/D0GC03226C>.
- 993 [16] D.E. Richardson, W.D. Raverty, Predicted environmental effects from liquid emissions
994 in the manufacture of levoglucosenone and Cyrene™, *Appita J.* (2016).
- 995 [17] F. Galiano, K. Briceño, T. Marino, A. Molino, K.V. Christensen, A. Figoli, Advances
996 in biopolymer-based membrane preparation and applications, *J. Memb. Sci.* 564 (2018)
997 562–586. <https://doi.org/10.1016/j.memsci.2018.07.059>.
- 998 [18] A. Iulianelli, F. Russo, F. Galiano, G. Desiderio, A. Basile, A. Figoli, PLA Easy Fil –
999 White-based membranes for CO₂ separation, *Greenh. Gases Sci. Technol.* 9 (2019)
1000 360–369. <https://doi.org/10.1002/ghg.1853>.
- 1001 [19] V. Ghaffarian, S.M. Mousavi, M. Bahreini, H. Jalaei, Polyethersulfone/poly (butylene
1002 succinate) membrane: Effect of preparation conditions on properties and performance,
1003 *J. Ind. Eng. Chem.* 20 (2014) 1359–1366. <https://doi.org/10.1016/j.jiec.2013.07.019>.
- 1004 [20] P. Tomietto, P. Loulergue, L. Paugam, J.-L. Audic, Biobased polyhydroxyalkanoate
1005 (PHA) membranes: structure/performances relationship, *Sep. Purif. Technol.* (2020)
1006 117419. <https://doi.org/10.1016/j.seppur.2020.117419>.
- 1007 [21] P. Tomietto, M. Carré, P. Loulergue, L. Paugam, J.-L. Audic, Polyhydroxyalkanoate
1008 (PHA) based microfiltration membranes: Tailoring the structure by the non-solvent
1009 induced phase separation (NIPS) process, *Polymer (Guildf.)* (2020) 122813.
1010 <https://doi.org/10.1016/j.polymer.2020.122813>.
- 1011 [22] P. Tomietto, P. Loulergue, L. Paugam, J.L. Audic, Polyhydroxyalkanoates (PHAs) for

- 1012 the Fabrication of Filtration Membranes, in: *Membr. Technol. Enhanc. Environ. Prot.*
1013 *Sustain. Ind. Growth*, Springer Nature, 2021: pp. 177–195. [https://doi.org/10.1007/978-](https://doi.org/10.1007/978-3-030-41295-1_11)
1014 [3-030-41295-1_11](https://doi.org/10.1007/978-3-030-41295-1_11).
- 1015 [23] S. Salerno, M.P. De Santo, E. Drioli, L. De Bartolo, Nano- and Micro-Porous Chitosan
1016 Membranes for Human Epidermal Stratification and Differentiation, *Membranes*
1017 (Basel). 11 (2021) 394. <https://doi.org/10.3390/membranes11060394>.
- 1018 [24] W. Xie, A. Tiraferri, B. Liu, P. Tang, F. Wang, S. Chen, A. Figoli, L.Y. Chu, First
1019 Exploration on a Poly(vinyl chloride) Ultrafiltration Membrane Prepared by Using the
1020 Sustainable Green Solvent PolarClean, *ACS Sustain. Chem. Eng.* (2020).
1021 <https://doi.org/10.1021/acssuschemeng.9b04287>.
- 1022 [25] R.J. Lee, Z.A. Jawad, A.L. Ahmad, H.B. Chua, Incorporation of functionalized multi-
1023 walled carbon nanotubes (MWCNTs) into cellulose acetate butyrate (CAB) polymeric
1024 matrix to improve the CO₂/N₂ separation, *Process Saf. Environ. Prot.* (2018).
1025 <https://doi.org/10.1016/j.psep.2018.04.021>.
- 1026 [26] F. Liu, B. Qin, L. He, R. Song, Novel starch/chitosan blending membrane:
1027 Antibacterial, permeable and mechanical properties, *Carbohydr. Polym.* 78 (2009)
1028 146–150. <https://doi.org/10.1016/j.carbpol.2009.03.021>.
- 1029 [27] G.-Q. Chen, A microbial polyhydroxyalkanoates (PHA) based bio- and materials
1030 industry, *Chem. Soc. Rev.* 38 (2009) 2434. <https://doi.org/10.1039/b812677c>.
- 1031 [28] S. Modi, K. Koelling, Y. Vodovotz, Assessment of PHB with varying hydroxyvalerate
1032 content for potential packaging applications, *Eur. Polym. J.* 47 (2011) 179–186.
1033 <https://doi.org/10.1016/j.eurpolymj.2010.11.010>.
- 1034 [29] Y.M. Corre, S. Bruzaud, J.L. Audic, Y. Grohens, Morphology and functional properties

- 1035 of commercial polyhydroxyalkanoates: A comprehensive and comparative study,
1036 Polym. Test. 31 (2012) 226–235. <https://doi.org/10.1016/j.polymertesting.2011.11.002>.
- 1037 [30] F.S. Poletto, L.A. Fiel, B. Donida, M.I. Ré, S.S. Guterres, A.R. Pohlmann, Controlling
1038 the size of poly(hydroxybutyrate-co-hydroxyvalerate) nanoparticles prepared by
1039 emulsification–diffusion technique using ethanol as surface agent, Colloids Surfaces A
1040 Physicochem. Eng. Asp. 324 (2008) 105–112.
1041 <https://doi.org/10.1016/j.colsurfa.2008.04.003>.
- 1042 [31] M.L. Tebaldi, A.L.C. Maia, F. Poletto, F.V. de Andrade, D.C.F. Soares, Poly(-3-
1043 hydroxybutyrate-co-3-hydroxyvalerate) (PHBV): Current advances in synthesis
1044 methodologies, antitumor applications and biocompatibility, J. Drug Deliv. Sci.
1045 Technol. 51 (2019) 115–126. <https://doi.org/10.1016/j.jddst.2019.02.007>.
- 1046 [32] J. Murray, J. Clark, T. Duncan, CYRENE: A new bio-based dipolar aprotic solvent., in:
1047 Green Chem. Eng. Conf. Portland, OR, United States, June 18-20, 2018.
- 1048 [33] J. Sherwood, M. De bruyn, A. Constantinou, L. Moity, C.R. McElroy, T.J. Farmer, T.
1049 Duncan, W. Raverty, A.J. Hunt, J.H. Clark, Dihydrolevoglucosenone (Cyrene) as a
1050 bio-based alternative for dipolar aprotic solvents, Chem. Commun. (2014).
1051 <https://doi.org/10.1039/c4cc04133j>.
- 1052 [34] T. Marino, F. Galiano, A. Molino, A. Figoli, New frontiers in sustainable membrane
1053 preparation: CyreneTM as green bioderived solvent, J. Memb. Sci. 580 (2019) 224–234.
1054 <https://doi.org/10.1016/j.memsci.2019.03.034>.
- 1055 [35] J.-L. Audic, L. Lemiègre, Y. Corre, Thermal and Mechanical Properties of a
1056 Polyhydroxyalkanoate Plasticized with Biobased Epoxidized Broccoli Oil, J. Appl.
1057 Polym. Sci. 39983 (2013) 1–7. <https://doi.org/10.1002/app.39983>.

- 1058 [36] J. Geens, B. Van der Bruggen, C. Vandecasteele, Characterisation of the solvent
1059 stability of polymeric nanofiltration membranes by measurement of contact angles and
1060 swelling, *Chem. Eng. Sci.* 59 (2004) 1161–1164.
1061 <https://doi.org/10.1016/j.ces.2004.01.003>.
- 1062 [37] S. Sawada, C. Ursino, F. Galiano, S. Simone, E. Drioli, A. Figoli, Effect of citrate-
1063 based non-toxic solvents on poly(vinylidene fluoride) membrane preparation via
1064 thermally induced phase separation, *J. Memb. Sci.* 493 (2015) 232–242.
1065 <https://doi.org/10.1016/j.memsci.2015.07.003>.
- 1066 [38] J.Y. Lai, F.C. Lin, C.C. Wang, D.M. Wang, Effect of nonsolvent additives on the
1067 porosity and morphology of asymmetric TPX membranes, *J. Memb. Sci.* 118 (1996)
1068 49–61. [https://doi.org/10.1016/0376-7388\(96\)00084-1](https://doi.org/10.1016/0376-7388(96)00084-1).
- 1069 [39] C.A. Smolders, A.J. Reuvers, R.M. Boom, I.M. Wienk, Microstructures in phase-
1070 inversion membranes. Part 1. Formation of macrovoids, *J. Memb. Sci.* 73 (1992) 259–
1071 275. [https://doi.org/10.1016/0376-7388\(92\)80134-6](https://doi.org/10.1016/0376-7388(92)80134-6).
- 1072 [40] B.S. Lalia, E. Guillen-Burrieza, H.A. Arafat, R. Hashaikeh, Fabrication and
1073 characterization of polyvinylidene fluoride-co-hexafluoropropylene (PVDF-HFP)
1074 electrospun membranes for direct contact membrane distillation, *J. Memb. Sci.* 428
1075 (2013) 104–115. <https://doi.org/10.1016/j.memsci.2012.10.061>.
- 1076 [41] J.T. Jung, J.F. Kim, H.H. Wang, E. di Nicolo, E. Drioli, Y.M. Lee, Understanding the
1077 non-solvent induced phase separation (NIPS) effect during the fabrication of
1078 microporous PVDF membranes via thermally induced phase separation (TIPS), *J.*
1079 *Memb. Sci.* 514 (2016) 250–263. <https://doi.org/10.1016/j.memsci.2016.04.069>.
- 1080 [42] T.H. Young, L.P. Cheng, D.J. Lin, L. Fane, W.Y. Chuang, Mechanisms of PVDF
1081 membrane formation by immersion-precipitation in soft (1-octanol) and harsh (water)

- 1082 nonsolvents, *Polymer (Guildf)*. 40 (1999) 5315–5323. <https://doi.org/10.1016/S0032->
1083 3861(98)00747-2.
- 1084 [43] J. Yang, D.W. Li, Y.K. Lin, X.L. Wang, F. Tian, Z. Wang, Formation of a
1085 bicontinuous structure membrane of polyvinylidene fluoride in diphenyl ketone diluent
1086 via thermally induced phase separation, *J. Appl. Polym. Sci.* 110 (2008) 341–347.
1087 <https://doi.org/10.1002/app.28606>.
- 1088 [44] N. Ismail, A. Venault, J.-P. Mikkola, D. Bouyer, E. Drioli, N. Tavajohi Hassan Kiadeh,
1089 Investigating the potential of membranes formed by the vapor induced phase separation
1090 process, *J. Memb. Sci.* 597 (2020) 117601.
1091 <https://doi.org/10.1016/j.memsci.2019.117601>.
- 1092 [45] T. Phaechamud, S. Chitrattha, Pore formation mechanism of porous poly(dl-lactic acid)
1093 matrix membrane, *Mater. Sci. Eng. C*. 61 (2016) 744–752.
1094 <https://doi.org/10.1016/j.msec.2016.01.014>.
- 1095 [46] P. Menut, C. Dupuy, Poly(ether imide) membrane formation by water vapour induced
1096 phase inversion, *Macromol. Symp.* 188 (2002) 37–48. <https://doi.org/10.1002/1521->
1097 3900(200211)188.
- 1098 [47] R.S. Hebbar, A.M. Isloor, A.F. Ismail, Contact Angle Measurements, in: *Membr.*
1099 *Charact.*, Elsevier, 2017: pp. 219–255. <https://doi.org/10.1016/B978-0-444-63776->
1100 5.00012-7.
- 1101 [48] A. Figoli, C. Ursino, F. Galiano, E. Di Nicolò, P. Campanelli, M.C. Carnevale, A.
1102 Criscuoli, Innovative hydrophobic coating of perfluoropolyether (PFPE) on
1103 commercial hydrophilic membranes for DCMD application, *J. Memb. Sci.* 522 (2017)
1104 192–201. <https://doi.org/10.1016/j.memsci.2016.08.066>.

- 1105 [49] D. Quéré, Rough ideas on wetting, in: *Phys. A Stat. Mech. Its Appl.*, 2002.
1106 [https://doi.org/10.1016/S0378-4371\(02\)01033-6](https://doi.org/10.1016/S0378-4371(02)01033-6).
- 1107 [50] Y. Wang, Y. Ke, L. Ren, G. Wu, X. Chen, Q. Zhao, Surface engineering of PHBV by
1108 covalent collagen immobilization to improve cell compatibility, *J. Biomed. Mater. Res.*
1109 *Part A.* 88A (2009) 616–627. <https://doi.org/10.1002/jbm.a.31858>.
- 1110 [51] L.-Y. Wang, Y.-J. Wang, D.-R. Cao, Surface Modification of Poly(3-hydroxybutyrate-
1111 co -3-hydroxyvalerate) Membrane by Combining Surface Aminolysis Treatment with
1112 Collagen Immobilization, *J. Macromol. Sci. Part A.* 46 (2009) 765–773.
1113 <https://doi.org/10.1080/10601320903004517>.
- 1114 [52] C.-K. Chang, H.-M. Wang, J. Lan, Investigation and Characterization of Plasma-
1115 Treated Poly(3-hydroxybutyrate) and Poly(3-hydroxybutyrate-co-3-hydroxyvalerate)
1116 Biopolymers for an In Vitro Cellular Study of Mouse Adipose-Derived Stem Cells,
1117 *Polymers (Basel)*. 10 (2018) 355. <https://doi.org/10.3390/polym10040355>.
- 1118 [53] A. Venault, A.J. Jumao-as-Leyba, Z.R. Yang, S. Carretier, Y. Chang, Formation
1119 mechanisms of low-biofouling PVDF/F127 membranes prepared by VIPS process, *J.*
1120 *Taiwan Inst. Chem. Eng.* 62 (2016) 297–306.
1121 <https://doi.org/10.1016/j.jtice.2015.12.033>.
- 1122 [54] Y. Ma, F. Shi, J. Ma, M. Wu, J. Zhang, C. Gao, Effect of PEG additive on the
1123 morphology and performance of polysulfone ultrafiltration membranes, *Desalination*.
1124 272 (2011) 51–58. <https://doi.org/10.1016/J.DESAL.2010.12.054>.
- 1125 [55] Q. Zhao, R. Xie, F. Luo, Y. Faraj, Z. Liu, X.J. Ju, W. Wang, L.Y. Chu, Preparation of
1126 high strength poly(vinylidene fluoride) porous membranes with cellular structure via
1127 vapor-induced phase separation, *J. Memb. Sci.* (2018).
1128 <https://doi.org/10.1016/j.memsci.2017.10.068>.

- 1129 [56] E. Bugnicourt, P. Cinelli, A. Lazzeri, V. Alvarez, Polyhydroxyalkanoate (PHA):
1130 Review of synthesis, characteristics, processing and potential applications in
1131 packaging, *Express Polym. Lett.* 8 (2014) 791–808.
1132 <https://doi.org/10.3144/expresspolymlett.2014.82>.
- 1133 [57] M.L. Di Lorenzo, M. Gazzano, M.C. Righetti, The role of the rigid amorphous fraction
1134 on cold crystallization of poly(3-hydroxybutyrate), *Macromolecules*. 45 (2012) 5684–
1135 5691. <https://doi.org/10.1021/ma3010907>.
- 1136 [58] L. Gzara, Z.A. Rehan, S. Simone, F. Galiano, N.T. Hassankiadeh, S.F. Al-Sharif, A.
1137 Figoli, E. Drioli, Tailoring PES membrane morphology and properties via selected
1138 preparation parameters, *J. Polym. Eng.* 37 (2017) 69–81.
1139 <https://doi.org/10.1515/polyeng-2015-0419>.
- 1140 [59] R.A. Milescu, C.R. Mcelroy, T.J. Farmer, P.M. Williams, M.J. Walters, J.H. Clark, Z.
1141 Xie, Fabrication of PES/PVP Water Filtration Membranes Using Cyrene, a Safer Bio-
1142 Based Polar Aprotic Solvent, *Adv. Microb. Physiol.* (2019).
1143 <https://doi.org/10.1155/2019/9692859>.
- 1144 [60] G.R. Guillen, G.Z. Ramon, H.P. Kavehpour, R.B. Kaner, E.M.V. Hoek, Direct
1145 microscopic observation of membrane formation by nonsolvent induced phase
1146 separation, *J. Memb. Sci.* 431 (2013) 212–220.
1147 <https://doi.org/10.1016/j.memsci.2012.12.031>.
- 1148 [61] A.B.D. Cassie, S. Baxter, Wettability of porous surfaces, *Trans. Faraday Soc.* 40
1149 (1944) 546. <https://doi.org/10.1039/tf94444000546>.
- 1150 [62] D. Wang, K. Li, W.K. Teo, Preparation and characterization of polyvinylidene fluoride
1151 (PVDF) hollow fiber membranes, *J. Memb. Sci.* 163 (1999) 211–220.
1152 [https://doi.org/10.1016/S0376-7388\(99\)00181-7](https://doi.org/10.1016/S0376-7388(99)00181-7).

- 1153 [63] M.G. Buonomenna, P. Macchi, M. Davoli, E. Drioli, Poly(vinylidene fluoride)
1154 membranes by phase inversion: the role the casting and coagulation conditions play in
1155 their morphology, crystalline structure and properties, *Eur. Polym. J.* 43 (2007) 1557–
1156 1572. <https://doi.org/10.1016/j.eurpolymj.2006.12.033>.
- 1157 [64] A. Bottino, G. Capannelli, S. Munari, A. Turturro, High performance ultrafiltration
1158 membranes cast from LiCl doped solutions, *Desalination*. 68 (1988) 167–177.
1159 [https://doi.org/10.1016/0011-9164\(88\)80052-3](https://doi.org/10.1016/0011-9164(88)80052-3).
- 1160 [65] M.J. Han, S.T. Nam, Thermodynamic and rheological variation in polysulfone solution
1161 by PVP and its effect in the preparation of phase inversion membrane, *J. Memb. Sci.*
1162 202 (2002) 55–61. [https://doi.org/10.1016/S0376-7388\(01\)00718-9](https://doi.org/10.1016/S0376-7388(01)00718-9).
- 1163 [66] W.-L. Chou, D.-G. Yu, M.-C. Yang, C.-H. Jou, Effect of molecular weight and
1164 concentration of PEG additives on morphology and permeation performance of
1165 cellulose acetate hollow fibers, *Sep. Purif. Technol.* 57 (2007) 209–219.
1166 <https://doi.org/10.1016/j.seppur.2007.04.005>.
- 1167 [67] M. Amirilargani, T. Mohammadi, Effects of PEG on morphology and permeation
1168 properties of polyethersulfone membranes, *Sep. Sci. Technol.* 44 (2009) 3854–3875.
1169 <https://doi.org/10.1080/01496390903182347>.
- 1170 [68] M. Villegas, A.I. Romero, M.L. Parentis, E.F. Castro Vidaurre, J.C. Gottifredi, Acrylic
1171 acid plasma polymerized poly(3-hydroxybutyrate) membranes for methanol/MTBE
1172 separation by pervaporation, *Chem. Eng. Res. Des.* 109 (2016) 234–248.
1173 <https://doi.org/10.1016/j.cherd.2016.01.018>.
- 1174 [69] M. Winterberg, E. Schulte-Körne, U. Peters, F. Nierlich, Methyl Tert -Butyl Ether, in:
1175 *Ullmann's Encycl. Ind. Chem.*, Wiley-VCH Verlag GmbH & Co. KGaA, Weinheim,
1176 Germany, 2010. https://doi.org/10.1002/14356007.a16_543.pub2.

- 1177 [70] S. Zereszki, A. Figoli, S.S. Madaeni, S. Simone, M. Esmailinezhad, E. Drioli,
1178 Pervaporation separation of MeOH/MTBE mixtures with modified PEEK membrane:
1179 Effect of operating conditions, *J. Memb. Sci.* 371 (2011) 1–9.
1180 <https://doi.org/10.1016/j.memsci.2010.11.068>.
- 1181 [71] R. Castro-Muñoz, J. Buera-González, Ó. de la Iglesia, F. Galiano, V. Fíla, M.
1182 Malankowska, C. Rubio, A. Figoli, C. Téllez, J. Coronas, Towards the dehydration of
1183 ethanol using pervaporation cross-linked poly(vinyl alcohol)/graphene oxide
1184 membranes, *J. Memb. Sci.* 582 (2019) 423–434.
1185 <https://doi.org/10.1016/j.memsci.2019.03.076>.
- 1186 [72] H. Wu, X. Fang, X. Zhang, Z. Jiang, B. Li, X. Ma, Cellulose acetate-poly(N-vinyl-2-
1187 pyrrolidone) blend membrane for pervaporation separation of methanol/MTBE
1188 mixtures, *Sep. Purif. Technol.* 64 (2008) 183–191.
1189 <https://doi.org/10.1016/j.seppur.2008.09.013>.
- 1190 [73] S. Zereszki, A. Figoli, S.S. Madaeni, S. Simone, E. Drioli, Pervaporation separation of
1191 methanol/methyl tert-butyl ether with poly(lactic acid) membranes, *J. Appl. Polym.*
1192 *Sci.* 118 (2010) 1364–1371. <https://doi.org/10.1002/app.32340>.
- 1193 [74] K. Zhou, Q.G. Zhang, G.L. Han, A.M. Zhu, Q.L. Liu, Pervaporation of water-ethanol
1194 and methanol-MTBE mixtures using poly (vinyl alcohol)/cellulose acetate blended
1195 membranes, *J. Memb. Sci.* 448 (2013) 93–101.
1196 <https://doi.org/10.1016/j.memsci.2013.08.005>.
- 1197 [75] M. Peivasti, A. Madandar, T. Mohammadi, Effect of operating conditions on
1198 pervaporation of methanol/methyl tert-butyl ether mixtures, *Chem. Eng. Process.*
1199 *Process Intensif.* 47 (2008) 1069–1074. <https://doi.org/10.1016/j.cep.2007.08.005>.
- 1200 [76] M. Villegas, E.F. Castro, A.C. Habert, J.C. Gottifredi, Sorption and pervaporation with

- 1201 poly (3-hydroxybutyrate) membranes : methanol / methyl tertbutyl ether mixtures, J.
1202 Memb. Sci. 367 (2011) 103–109. <https://doi.org/10.1016/j.memsci.2010.10.051>.
- 1203 [77] R. Castro-Muñoz, F. Galiano, V. Fíla, E. Drioli, A. Figoli, Matrimid@5218 dense
1204 membrane for the separation of azeotropic MeOH-MTBE mixtures by pervaporation,
1205 Sep. Purif. Technol. 199 (2018) 27–36. <https://doi.org/10.1016/j.seppur.2018.01.045>.
- 1206 [78] P.-S. Mok, D. Hooi, E. Ch'ng, S.-P. Ong, K. Numata, K. Sudesh, Characterization of
1207 the depolymerizing activity of commercial lipases and detection of lipase-like activities
1208 in animal organ extracts using poly(3-hydroxybutyrate-co-4-hydroxybutyrate) thin
1209 film, AMB Express. (2016). <https://doi.org/10.1186/s13568-016-0230-z>.
- 1210 [79] P. Kanmani, J. Aravind, K. Kumaresan, An insight into microbial lipases and their
1211 environmental facet, Int. J. Environ. Sci. Technol. 12 (2015) 1147–1162.
1212 <https://doi.org/10.1007/s13762-014-0605-0>.
- 1213 [80] K. Mukai, K. Yamada, Y. Doi, Extracellular poly(hydroxyalkanoate) depolymerases
1214 and their inhibitor from *Pseudomonas lemoignei*, Int. J. Biol. Macromol. 14 (1992)
1215 235–239. [https://doi.org/10.1016/S0141-8130\(05\)80034-0](https://doi.org/10.1016/S0141-8130(05)80034-0).
- 1216 [81] D. Hooi, E. Ch'ng, K. Sudesh, Densitometry based microassay for the determination of
1217 lipase depolymerizing activity on polyhydroxyalkanoate, AMB Express. (2013).
- 1218 [82] N.A. Tarazona, R. Machatschek, A. Lendlein, Influence of Depolymerases and Lipases
1219 on the Degradation of Polyhydroxyalkanoates Determined in Langmuir Degradation
1220 Studies, Adv. Mater. Interfaces. 7 (2020) 2000872.
1221 <https://doi.org/10.1002/admi.202000872>.
- 1222 [83] J. Han, L.-P. Wu, X.-B. Liu, J. Hou, L.-L. Zhao, J.-Y. Chen, D.-H. Zhao, H. Xiang,
1223 Biodegradation and biocompatibility of haloarchaea-produced poly(3-hydroxybutyrate-

1224 co-3-hydroxyvalerate) copolymers, *Biomaterials*. 139 (2017) 172–186.
1225 <https://doi.org/10.1016/j.biomaterials.2017.06.006>.

1226 [84] M. Deroiné, G. César, A. Le Duigou, P. Davies, S. Bruzard, Natural Degradation and
1227 Biodegradation of Poly(3-Hydroxybutyrate-co-3-Hydroxyvalerate) in Liquid and Solid
1228 Marine Environments, *J. Polym. Environ.* 23 (2015) 493–505.
1229 <https://doi.org/10.1007/s10924-015-0736-5>.

1230 [85] A.N. Boyandin, V.P. Rudnev, V.N. Ivonin, S. V. Prudnikova, K.I. Korobikhina, M.L.
1231 Filipenko, T.G. Volova, A.J. Sinsky, Biodegradation of Polyhydroxyalkanoate Films
1232 in Natural Environments, *Macromol. Symp.* 320 (2012) 38–42.
1233 <https://doi.org/10.1002/masy.201251004>.

1234 [86] H. Tsuji, K. Suzuyoshi, Environmental degradation of biodegradable polyesters 1.
1235 Poly(ϵ -caprolactone), poly[(R)-3-hydroxybutyrate], and poly(L-lactide) films in
1236 controlled static seawater, *Polym. Degrad. Stab.* 75 (2002) 347–355.
1237 [https://doi.org/10.1016/S0141-3910\(01\)00240-3](https://doi.org/10.1016/S0141-3910(01)00240-3).

1238 [87] M. Rutkowska, A.E. Katarzyna, K. Ae, A. Heimowska, A.E. Gra_Zyna Adamus, A.E.
1239 Michał, S. Ae, M. Musioł, A.E. Henryk, J. Ae, W. Sikorska, A.E. Andrej, K. Ae, E.Z.˘
1240 A. Ae, M. Kowalczyk, Environmental Degradation of Blends of Atactic Poly[(R,S)-3-
1241 hydroxybutyrate] with Natural PHBV in Baltic Sea Water and Compost with Activated
1242 Sludge, *J. Polym. Environ.* 16 (2008) 183–191. [https://doi.org/10.1007/s10924-008-](https://doi.org/10.1007/s10924-008-0100-0)
1243 [0100-0](https://doi.org/10.1007/s10924-008-0100-0).

1244

1245